Chapter VI

THE CDG ANALYSIS METHOD

VI.A. Overview

We assume that the CDG radiation is isotropic in space and constant in time. As such there is no unique spatial or temporal signature of the CDG signal in the data to aid in its identification and ultimate separation. The CDG measurement is made by subtracting every instrumental background source, terrestrial sources and then attributing the remaining flux to the CDG radiation.

The best data to study the CDG intensity are those from high-latitude viewing periods (see section IV.A). In addition, we use observation times when the Earth is completely outside the COMPTEL field-of-view (see section IV.B). These selections suppress the effect of the diffuse Galactic emission and the contribution from the Earth's atmosphere.

In constructing the CDG spectrum, the first step is to determine the forward-peak count rates, using standard-CDG data selections, by fitting the time-of-flight (ToF) spectrum with components as described in section V.A. The forward peak contains the counts due to the CDG radiation. The ToF fit separates the background events in the ToF spectrum. The internal background events within the forward-peak must be removed before arriving at the count rate due to the CDG radiation.

For each bin in total energy, the fitted ToF forward-peak count rates are ordered by the instantaneous veto rates to construct veto growth curves (VGCs) (see section V.E). Above 4.2 MeV, in the absence of long-lived background, the fitted ToF-peak rates consists of only the CDG and the prompt background components. Since the veto signals are dominated by charged cosmic rays, a zero veto rate corresponds to zero cosmic-ray intensity. The 2.223 MeV line rate, prompt in nature, is proportional to the veto rate. Hence, the prompt background is assumed to vary linearly with the veto rate and extrapolate to zero at zero veto

rate (see section V.E for a detailed discussion of VGCs and the prompt background). Therefore, above 4.2 MeV, the ToF-peak VGCs are fitted by a straight line to extrapolate the ToF-peak rates to zero veto rate. The extrapolated event rate at zero veto rate is the CDG count rate.

Long-lived background events are due to de-excitation photons from radioactive isotopes with long half-lives ($\tau_{1/2}$ > 1 minute). As a result of the long half-lives, the background rate depends on the activation history (primarily the SAA dose) and the particular isotope half-life, but is *not* related to the instantaneous cosmic-ray intensity. Because of the varied activation over the mission lifetime and the addition of data from different periods in the CDG analysis, the behavior of the long-lived component is complex. We use the measured spectrum (ETOT and E2) to identify isotope decays. Monte Carlo simulations determine the COMPTEL response to each isotope decay. The absolute contribution of each of the long-lived background isotopes is determined by fitting the energy spectra with the response from Monte Carlo simulation (see section V.C for a detailed discussion of the long-lived background).

Below 4.2 MeV, the ToF-peak rates consist of long-lived background events in addition to the CDG and prompt background components. For energy bins below 4.2 MeV, we first compute the contributions of each long-lived isotope in each veto bin. We subtract the long-lived contributions of each isotope from the ToF-peak VGCs for each veto bin. After the long-lived background subtractions, the resulting VGCs consist of only the CDG and the prompt background components. Now, as in the case above 4.2 MeV, the VGCs are fit to a straight line to determine the CDG count rate at zero veto rate.

The CDG flux is then determined by deconvolving the resultant CDG count spectrum. The instrument response to a diffuse source is determined from Monte Carlo simulations of a diffuse isotropic source, with a power-law distribution in energy, propagated through a detailed COMPTEL mass model (see section II.E).

There are three distinct energy intervals that have its unique background features, namely, the 9–30, 4.2–9 and 0.8–4.2 MeV intervals. The CDG analysis is tailored separately for each distinct energy interval. The CDG analysis is performed for 9 separate total energy intervals

with boundaries at 0.8, 1.2, 1.8, 2.7, 4.2, 6, 9, 12, 17 and 30 MeV. The bin boundaries at 6, 12 and 17 MeV were chosen to more evenly distribute the counts above 4.2 MeV. The energy intervals below 4.2 MeV are chosen so as to encompass strong long-lived activation lines within them. The 2.7–4.2 MeV region is dominated by ^{24}Na decay, the 1.8–2.7 MeV region contains the 2.223 MeV line and the ^{28}Al decay, while the 1.2–1.8 MeV region contains the 1.4 MeV line from ^{40}K and the ^{22}Na decay.

For a given total energy range, the distribution of D1 and D2 energy deposits for external-photon type A events are different from those for internal-multiple-photon type C events. This translates into a difference in the measured ϕ angles for type A events and type C events. Hence, in certain energy ranges we can further optimize for the CDG signal by making an additional ϕ selection. Since the background is simplest at the highest energies and becomes increasingly complicated as one moves to lower energies, I will start by discussing the analysis and results for the higher energies and will progress to the lower energies.

VI.B. The 9–30 MeV CDG Analysis

The 9 to 30 MeV region represents the cleanest energy regime in the COMPTEL dataspace. At these energies the ToF-peak has the highest signal-to-background ratio and dominates the count spectrum in the 110–130 ToF range. Above 9 MeV, the ToF peak counts consist of only the prompt background and the CDG radiation. The prompt background events are present near the expected scattered-photon peak at channel 120 in ToF, suggesting that the background events above ~9 MeV are type A events.

VI.B.1 The ToF Spectrum

The ToF spectra above 9 MeV are fit by the Exponential-ToF model. The forward-peak is modeled as a single gaussian superimposed over a continuum consisting of an exponential and a constant. In each energy bin, the gaussian-position, gaussian-width and exponential-curvature are fixed for all fits. This reduces the number of free parameters to better constrain the fit parameters; namely the gaussian amplitude, the exponential normalization and the constant level. The fixed parameters are not influenced by the veto rates (see section V.D). The ToF-peak counts are then divided by the appropriate livetime for that veto rate to get the

ToF-peak count rate. The ToF spectrum summed over all veto bins for the P12345 Virgo data in the 9–12, 12–17 and 17–30 MeV bins are shown in figures VI.B.1 and VI.B.2.

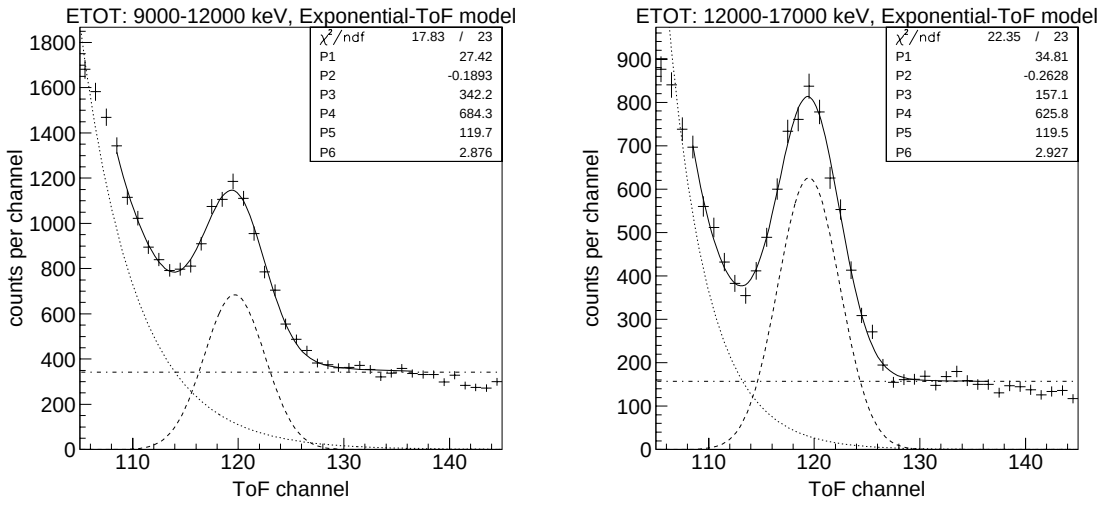

(a) (b)

Figure VI.B.1 The (a) 9–12 and (b) 12–17 MeV ToF spectrum with standard-CDG selections for Virgo data.

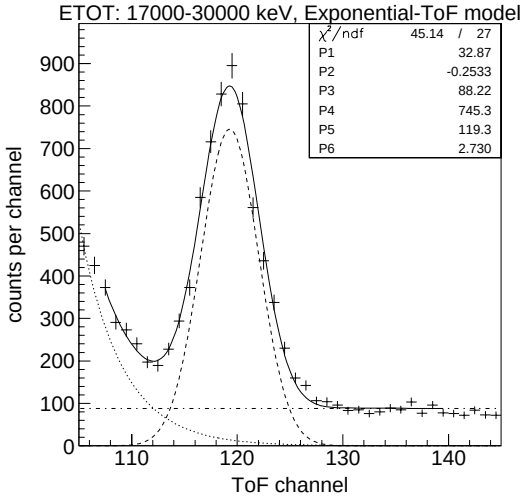

Figure VI.B.2 The 17–30 MeV ToF spectrum with standard-CDG selections for Virgo data.

VI.B.2 The VGC Modulation

The ToF-peak VGCs are then fit by a straight line. The constant (*y*-intercept) event rate is the CDG count rate. The slope is a measure of the prompt background. For the following discussion we define some useful ratios.

♦ Modulation factor M_v as the ratio of the event rate at the highest veto bin ($Rate_{v2:2000}$) over the event rate at the lowest veto bin ($Rate_{veto:650}$) for a given VGC. The measured M_v is an indicator of the dynamic range (or sensitivity) of COMPTEL to the prompt background. The modulation factor is typically about 2.4 in the 9 to 30 MeV range.

♦ Signal-to-background ratio (S/B) as the ratio of the CDG event rate ($Rate_{CDG}$) over the event rate at the lowest veto bin ($Rate_{veto:650}$) for a given VGC. Since $Rate_{veto:650}$ has the lowest prompt component, the S/B ratio gives the largest fraction of measured CDG counts prior to any prompt or long-lived background correction. The measured S/B ratio is around 25–40% in the 9 to 30 MeV range.

Table V1.B.1 The M_v and S/B ratios for the Virgo and SGP datasets above 9 MeV.

Energy	Event rate (counts/s)			Modu-lation	S/B
(MeV)	veto2: 0 (CGD)	veto2: 650–800	veto2: 2000–2500	(M_v)	(%)
Virgo					
9–30	0.00134	0.00436	0.00989	2.27	32.3
9–12	0.000598	0.00152	0.00333	2.19	39.3
12–17	0.000499	0.00140	0.00318	2.27	35.6
17–30	0.000141	0.00142	0.00372	2.62	9.90
SGP					
9–30	0.000899	0.00370	0.00894	2.41	24.3
9–12	0.000548	0.00136	0.00276	2.04	40.4
12–17	0.000368	0.00110	0.00267	2.42	33.4
17–30	0.0000185	0.00116	0.00344	2.96	1.59

It is illustrative to examine these two ratios to appreciate the magnitude and dynamics of the prompt background. M_v is directly related to the slope of the VGC. The measured modulation factor is in the range of 2.2 to 2.7 in the 9 to 30 MeV range. M_v increases with energy above 9 MeV. For the P12345 Virgo data, M_v varies from 2.19 at 9–12 MeV to 2.65 at 17–30 MeV. The measured modulation factors agree with the results of Share et al. (Share, Kinzer, and Seeman 1974) where a modulation factor of about 2.3 was measured at similar energies using a spark-chamber instrument at balloon altitudes. The table VI.B.1 below shows the modulation factor and the S/B ratio for the Virgo and SGP data at energies above 9 MeV. The VGCs for the Virgo and SGP data are plotted with standard-CDG selection for the 9–12,

12–17 and 17–30 MeV bins in figures VI.B.3–5. The rate from the Virgo and SGP data are similar in each energy bin.

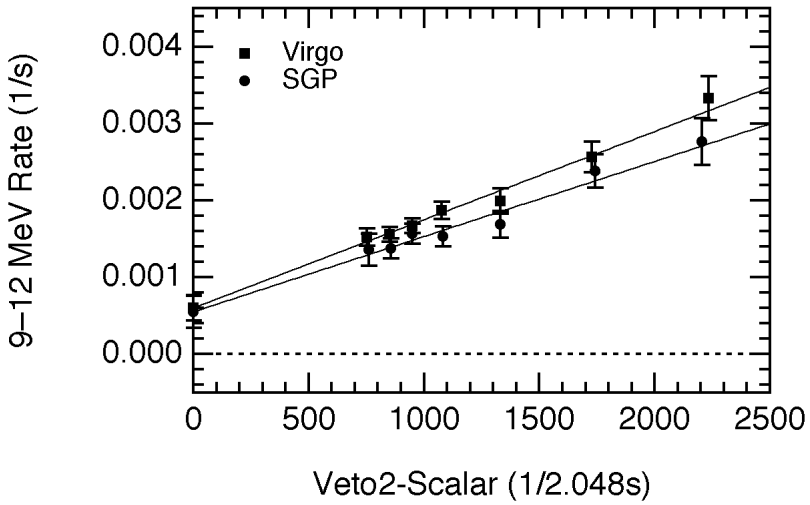

Figure VI.B.3 The 9–12 MeV VGC with standard-CDG selections for the Virgo and SGP observations.

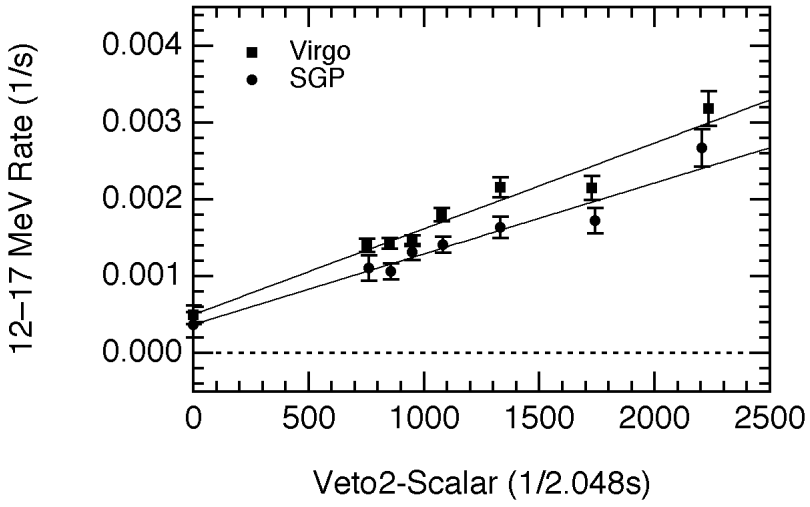

Figure VI.B.4 The 12–17 MeV VGC with standard-CDG selections for the Virgo and SGP observations.

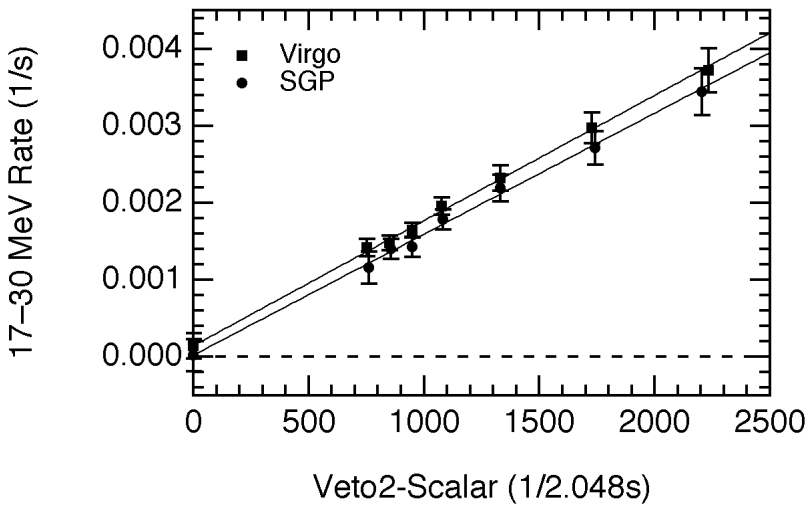

Figure VI.B.5 The 17–30 MeV VGC with standard-CDG selections for the Virgo and SGP observations.

VI.B.3 Phi 7–22˚ Selection for 17–30 MeV

The lower S/B is clearly seen in the 17–30 MeV bin. The fraction of the CDG signal in the 17–30 MeV bin is relatively low at ~10% compared to ~40% for the 9–12 and 12–17 MeV bins. The 17–30 MeV bin also has the largest veto modulation of 2.62 compared to 2.19 and 2.27 for the other bins, respectively.

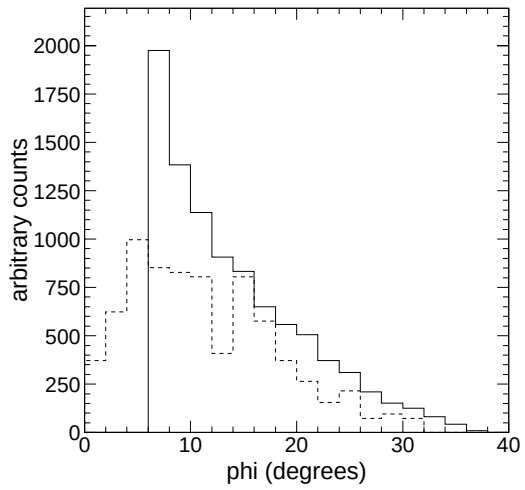

Figure VI.B.6 The 9–30 MeV ϕ spectrum of the data (solid) with the ϕ spectrum obtained from the CDG simulations (dashed) with arbitrary scaling.

Restricting the acceptable ϕ values to the range 7–22˚ from 6–38˚ improves the sensitivity in the 17–30 MeV range. This ϕ selection was chosen as a result of comparing the ϕ spectrum

of the data to the CDG simulations. In figure VI.B.6, the 9–30 MeV ϕ spectrum of the data and the ϕ spectrum obtained from the CDG simulations are plotted with arbitrary scaling. The figure shows that the ϕ spectra have different shapes. The simulated ϕ spectrum does not have the sharp rise at angles below 10˚ and seems to flatten out above 20˚. The CDG signal fraction is highest at low scatter angles.

The influence of the ϕ 7–22˚ selection can also be seen in its effect on $Rate_{v2:2000}$ (the count rate at veto2:2000-2500 bin) and A_{eff} (the instrument effective area). The table V1.B.2 below shows the relative decrease to A_{eff} and $Rate_{v2:2000}$ due to the new ϕ selection of 7–22˚ compared to the standard CDG ϕ selection of 6–38˚. The largest improvement is seen in the 17–30 MeV range where there is a ~30% decrease in $Rate_{v2:2000}$ but only a ~14% decrease in A_{eff} .

Table V1.B.3 The effect of the ϕ 7–22˚ selection on A_{eff} and $Rate_{v2:2000}$.

Energy (MeV)	Ratio of A_{eff}	Ratio of $Rate_{v2:2000}$
9-12	0.775	0.752
12-17	0.800	0.699
17-30	0.862	0.704

The table VI.B.3 shows the 17–30 MeV modulation factor and the S/B ratio for the Virgo and SGP data with the two different ϕ selections. The modulation M_v decreases with the ϕ 7–22˚ selection from 2.62 to 2.35 and S/B ratio increases from 9.9% to 22.2% for the Virgo data. The improvements are seen in the SGP data too but to a lesser degree where the S/B ratio increases from ~1.6% to ~8.8% for the ϕ 7–22˚ selection.

Table V1.B.4 Comparison between the M_v and S/B ratios for the Virgo and SGP datasets above 9 MeV for the two different ϕ selections.

Φ Selection	17–30 MeV Event rate (counts/s)			Modu-lation	S/B
	veto2: 0 (CGD)	veto2: 650–800	veto2: 2000–2500	(M_v)	(%)
Virgo					
ϕ 6-38˚	0.000141	0.00142	0.00372	2.62	9.90
ϕ 7-22˚	0.000243	0.00109	0.00257	2.35	22.22
SGP					
ϕ 6-38˚	0.0000185	0.00116	0.00344	2.96	1.59
ϕ 7-22˚	0.0000739	0.000836	0.00257	3.08	8.84

The CDG results with the ϕ 7–22˚ cut for the Virgo and the SGP data are shown in table VI.B.4 and VI.B.5. The changes in the computed CDG flux are not significant for the 9–12

and the 12–17 MeV bins. However, due to the increases S/B ratio, the ϕ 7-22° selection results in a higher detection significance of the 17–30 MeV CDG flux. The significance of the 17–30 MeV CDG flux detection increases from 1.23 to 2.55 σ for the Virgo data and from 0.12 to 0.57 σ for the SGP data.

Table V1.B.5 Comparison of the CDG flux for the two different ϕ selections above 9 MeV using the Virgo data

Energy (MeV)	CDG flux — Virgo data 10^{-5} (photons/cm^2-s-sr-MeV)	
	ϕ: 6–38°	ϕ: 7–22°
9–12	1.78 ± 0.48	1.84 ± 0.54
12–17	1.06 ± 0.27	1.23 ± 0.27
17–30	0.164 ± 0.133	0.327 ± 0.128

Table V1.B.6 Comparison of the CDG flux for the two different ϕ selections above 9 MeV using the SGP data.

Energy (MeV)	CDG flux — SGP data 10^{-5} (photons/cm^2-s-sr-MeV)	
	ϕ: 6–38°	ϕ: 7–22°
9–12	1.69 ± 0.64	1.66 ± 0.73
12–17	0.797 ± 0.350	0.488 ± 0.355
17–30	0.022 ± 0.180	0.103 ± 0.179

A comparison between the VGCs for the two different ϕ selections is shown in figure VI.B.7 for the 17–30 MeV Virgo data. The flattening of the VGC with the ϕ 7–22° selections is evident. The 17–30 MeV VGC for the Virgo and SGP observations with the ϕ selection of 7–22° is shown in figure VI.B.8. The rate from the Virgo and SGP data are consistent. Thus, the ϕ selection of 7–22° is the *optimized data selection* for the CDG analysis in the 17–30 MeV energy range, while the standard-CDG selection of ϕ 6–38° is adequate for the CDG analysis in the 9–12 and 12–17 MeV bins.

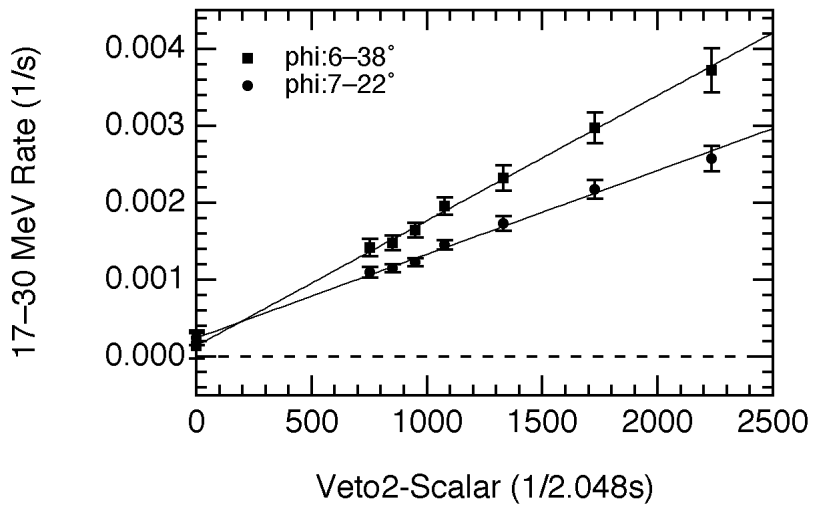

Figure VI.B.7 The Virgo 17–30 MeV VGC illustrating the impact of the two different ϕ selections.

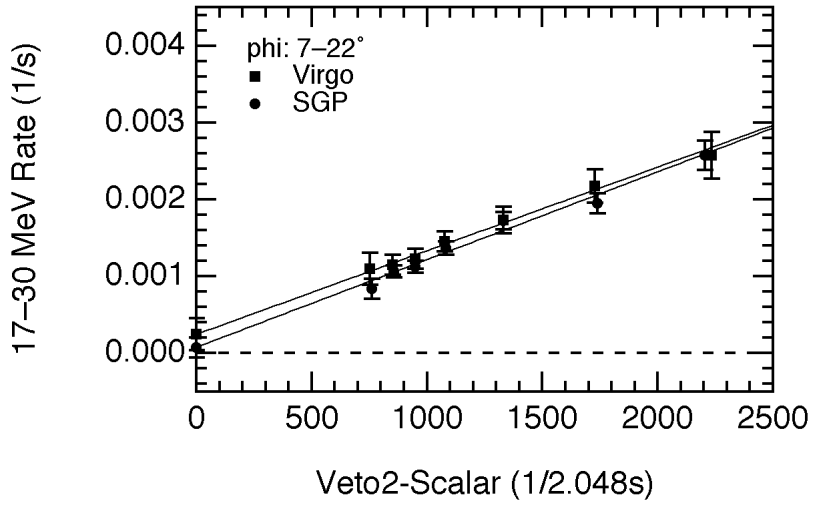

Figure VI.B.8 The 17–30 MeV VGC for the Virgo and SGP observations with ϕ 7–22˚ selection.

VI.B.4 The 9–30 MeV CDG Flux Calculation

The CDG flux has been derived using a linear extrapolation of the ToF-peak VGC with the appropriate ϕ selections in the 9–12, 12–17, and 17–30 MeV bins (i.e., ϕ 6–38˚ for the 9–12 and 12–17 MeV bins and ϕ 7–22˚ for the 17–30 MeV bin). The results are shown below in table VI.B.7 and VI.B.8 for the Virgo, SGP and combined datasets.

The total 9–30 MeV flux from the Virgo observations has a detection significance of 5.8σ and represents the first significant detection of the CDG flux in this energy range. The

CDG flux in the finer energy intervals of 9–12, 12–17 and 17–30 MeV have detection significances of 3.7, 4.0 and 2.6 σ, respectively.

The total 9–30 MeV flux from the SGP observations has a detection significance of 3.0 σ and is consistent with that from the Virgo direction. The CDG flux from the SGP observations has detection significances of 2.6, 2.3 and 0.6 σ in the finer energy intervals of 9–12, 12–17 and 17–30 MeV respectively. The CDG flux in 17–30 MeV interval from the SGP data is consistent with zero. The corresponding 2σ upper-limit is 4.6×10^{-6} (photons/cm^2-s-sr-MeV), where the 2σ upper-limit is defined as the measurement plus twice the 1σ statistical error.

The total CDG flux using the combined Phase I to Phase V Virgo and SGP data from 9 to 30 MeV is also shown in table VI.B.7. The CDG fluxes have detection significances of 7.2, 4.9, 5.3 and 2.7 σ for the 9–30, 9–12, 12–17 and 17–30 MeV intervals, respectively. For comparison, the 17–30 MeV CDG results derived using both the standard and optimized ϕ selection are shown below in table VI.B.8.

Table V1.B.7 The CDG rate and flux between 9 and 30 MeV († 2σ upper-limit).

Energy (MeV)	CGD Event-Rate $\times 10^{-4}$ (counts/s)	Effective-Area (cm^2-sr)	CDG Flux (1/cm^2-s-sr-MeV)
Virgo			
9–30	13.4 ± 2.3	9.42	$(6.8 \pm 1.2) \times 10^{-6}$
9–12	6.0 ± 1.6	11.2	$(1.8 \pm 0.5) \times 10^{-5}$
12–17	5.0 ± 1.3	9.45	$(1.1 \pm 0.3) \times 10^{-5}$
17–30	2.4 ± 0.9	5.67	$(3.3 \pm 1.3) \times 10^{-6}$
SGP			
9–30	9.0 ± 3.0	9.16	$(4.7 \pm 1.6) \times 10^{-6}$
9–12	5.5 ± 2.1	10.8	$(1.7 \pm 0.6) \times 10^{-5}$
12–17	3.7 ± 1.6	9.24	$(8.0 \pm 3.5) \times 10^{-6}$
17–30	0.7 ± 1.3	5.54	$4.6 \times 10^{-6\,\dagger}$
Virgo+SGP			
9–30	12.4 ± 1.7	9.33	$(6.3 \pm 0.9) \times 10^{-6}$
9–12	6.2 ± 1.3	11.1	$(1.8 \pm 0.4) \times 10^{-5}$
12–17	5.2 ± 1.0	9.37	$(1.1 \pm 0.2) \times 10^{-5}$
17–30	2.0 ± 0.7	5.63	$(2.8 \pm 1.0) \times 10^{-6}$

Table V1.B.8 A comparison between the 17–30 MeV CDG results derived using the two different ϕ selection († 2σ upper-limit).

Data	17–30 MeV CGD Rate $\times 10^{-4}$ (counts/s)	Effective-Area (cm^2-sr)	17–30 MeV CDG Flux $\times 10^{-6}$ (1/cm^2-s-sr-MeV)
ϕ: 7–22°			
Virgo+SGP	2.0 ± 0.7	5.63	2.8 ± 1.0
Virgo	2.4 ± 0.9	5.67	3.3 ± 1.3
SGP	0.7 ± 1.3	5.54	4.6†
ϕ: 6–38°			
Virgo+SGP	1.3 ± 0.9	6.53	1.5 ± 1.1
Virgo	1.4 ± 1.1	6.58	1.6 ± 1.3
SGP	0.2 ± 1.5	6.42	3.8†

VI.B.5 Consistency Check for the Analysis Method

A consistency check for the CDG analysis method in the 9 to 30 MeV range is to compare the CDG flux for subsets of the data. One can check if the results are consistent among subsets of the data, namely, the P12V, P3V, P45V, P1SGP and P45SGP datasets. To compensate for the decrease in statistics for five smaller data subsets, the CDG flux are computed for the total 9–30 MeV interval. The measured 9–30 MeV CDG fluxes for the five *independent* datasets together with their average value are shown in table VI.B.9 and plotted in figure VI.B.9. The ToF-peak VGCs for the five data subsets are shown in figure VI.B.10.

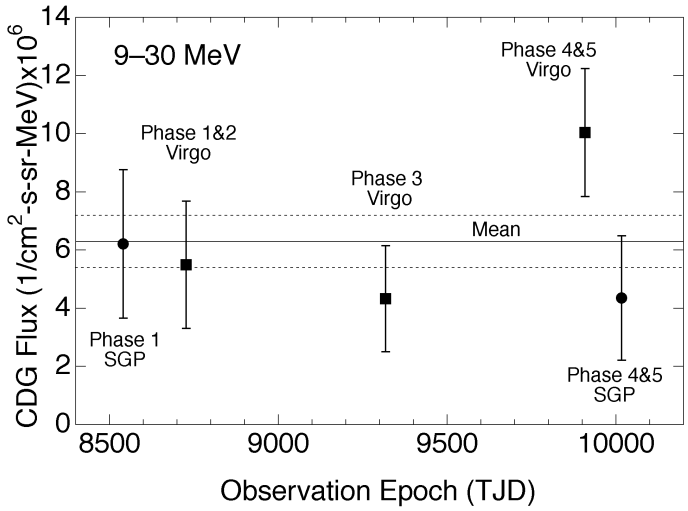

Figure VI.B.9 The measured 9–30 MeV CDG flux for the five independent datasets and the average flux together with its 1σ levels.

To test the consistency between the measurements, the five independent measurements were compared to the average value derived from the combined dataset, $(6.3 \pm 0.9) \times 10^{-6}$ (1/cm^2-s-sr-MeV). The reduced chi-square of the fit is 1.26. The null hypothesis of a constant

flux is rejected only at only the 70% confidence level. The five independent 9–30 MeV flux measurements are consistent with a constant CDG emission, suggesting that the analysis methods used are robust and reliable.

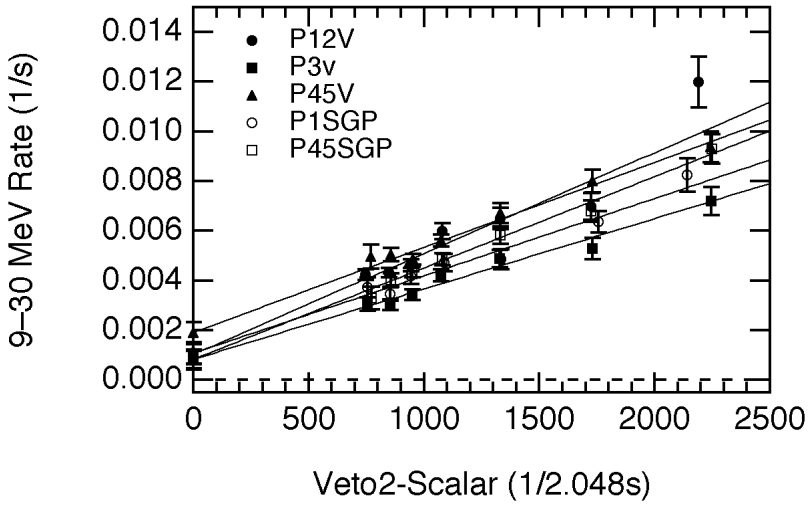

Figure VI.B.10 The 9–30 MeV VGC for the five independent datasets .

Table V1.B.9 The measured 9–30 MeV CDG flux for the five independent datasets.

Data	9–30 MeV CGD Rate $\times 10^{-4}$ (counts/s)	Effective-Area (cm^2-sr)	9–30 MeV CDG Flux $\times 10^{-6}$ ($1/cm^2$-s-sr-MeV)
Virgo+SGP	12.4 ± 1.7	9.33	6.3 ± 0.9
Virgo	13.4 ± 2.3	9.42	6.8 ± 1.2
SGP	9.0 ± 3.0	9.16	4.7 ± 1.6
mean V&S			5.9 ± 1.0
P12V	10.2 ± 4.1	9.30	5.5 ± 2.2
P3V	8.2 ± 3.5	9.49	4.3 ± 1.8
P45V	19.1 ± 4.2	9.49	10.0 ± 2.2
P1SGP	10.7 ± 4.4	8.64	6.2 ± 2.5
P45SGP	8.2 ± 4.1	9.49	4.4 ± 2.1

VI. C. The 4.2–9 MeV CDG Analysis

The 4.2–9 MeV region represents the next simplest energy regime in COMPTEL dataspace after the 9–30 MeV interval. Between 4.2 and 9 MeV the ToF peak counts consist of only the prompt background and the CDG radiation. However the nature of the background in the 4.2–9 MeV region is different from that at 9–30 MeV. Although the 4.2–9 MeV region contains prompt type A events as the 9–30 MeV interval, it also has a large fraction (~50%) of the forward-peak counts as prompt type C events originating near the D1 subsystem. While type A events nominally peak at channel 120, type C events are located at

lower ToF channels near channel 116. Due to the large fraction of type C events we have modified the ToF fit procedure to separate the peak at 120 (containing the signal) from the peak at ~116 (section V.D).

VI.C.1 The ToF Spectrum

The fits of the P15VSGP data in the 4.2–6 and 6–9 MeV bin with the 2gToF model for standard-CDG selections are shown in figures VI.C.1 and VI.C.2. Typically, the measured counts in the ToF peak at channel 120 are about 50–55% of the counts in the single ToF-peak at channel 118, a factor of 2 improvement in the S/B ratio. See section V.D for details on the 2gToF model.

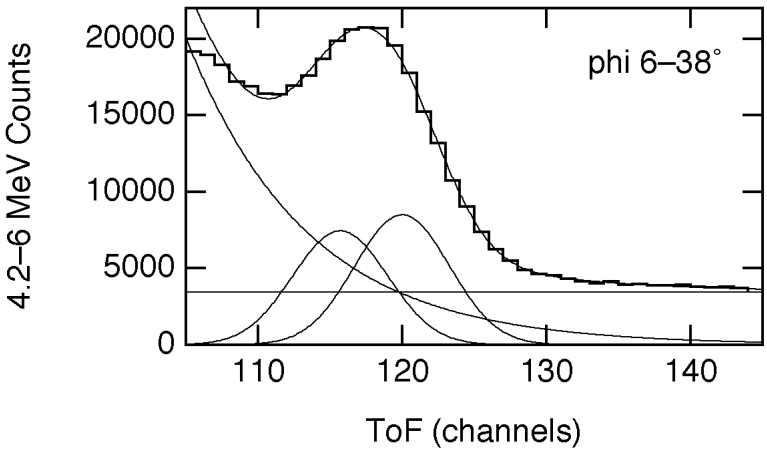

Figure VI.C.1 The 4.2–6 MeV all-veto P15VSGP ToF spectrum fit using the 2gToF model.

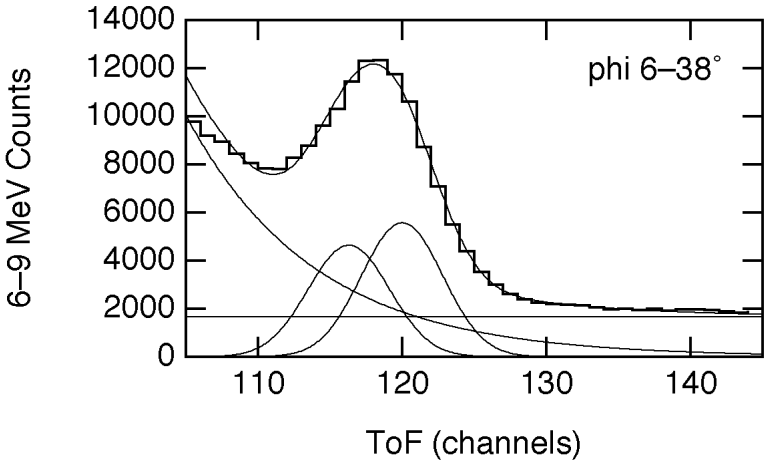

Figure VI.C.2 The 6–9 MeV all-veto P15VSGP ToF spectrum fit using the 2gToF model.

VI.C.2 Phi 18–38˚ Selection for 4.2–9 MeV

A ϕ selection of 18–38˚ improves the sensitivity in the 4.2–9 MeV range. Figure VI.C.3 shows the 4.2–9 MeV ϕ spectrum of the data and the simulations, arbitrary scaled to compare shapes. The ϕ spectra of the data and simulations have different shapes. The data peaks at ~6˚ (recall the data has the standard ϕ 6–38˚ selection) and decreases sharply with increasing ϕ. On the other hand, the simulation shows only a gradually decrease above 6˚. Such a difference in shape suggests that the CDG signal fraction is greatest at large scatter angles. Most events below 18˚ are probably internal background and should be rejected.

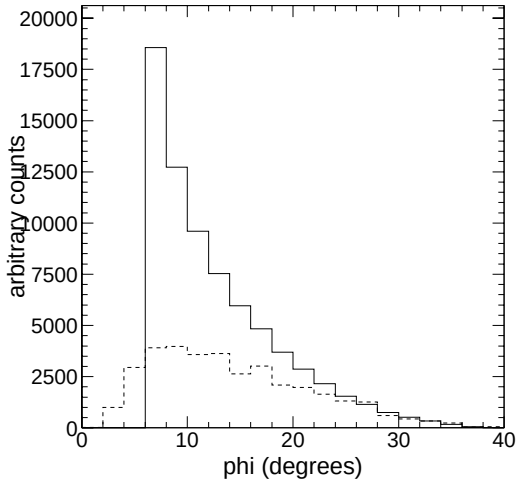

Figure VI.C.3 The 4.2–9 MeV ϕ spectrum of the data (solid) with the ϕ spectrum obtained from the CDG simulations (dashed) with arbitrary scaling.

Similar to the 9–30 MeV work in section VI.B, we have tabulated the relative changes to A_{eff} (the effective area) and $Rate_{v2:2000}$ (the count rate in the veto2:2000-2500 bin) for the ϕ selections of 18–38˚ and 6–38˚. For the ϕ 18–38˚ selection there are large changes in both quantities, but a significant improvement in the S/B ratio. Although A_{eff} drops by a factor of ~2.5, $Rate_{v2:2000}$ decreases by a factor of 4–5. This results in a factor of ~2 improvement in the S/B ratio. However, the overall count rates also decrease by 40–65%, slightly more than the decrease produced by the 2gToF fit (45–50%). The table VI.B.1 below shows the relative decrease to A_{eff} and $Rate_{v2:2000}$ due to the 18–38˚ ϕ selection compared to the same quantities for standard CDG ϕ selection of 6–38˚.

Table VI.C.1 The effect of the ϕ 18–38˚ selection on A_{eff} and $Rate_{v2:2000}$.

Energy (MeV)	Ratio of A_{eff}	Ratio of $Rate_{v2:2000}$
Virgo		
4.2–6	0.380	0.228
6–9	0.331	0.212
SGP		
4.2–6	0.379	0.232
6–9	0.334	0.234

We can now improve the S/B ratio in the 4.2–9 MeV measurements by (1) using the 2gToF model and (2) by applying a $\phi \geq 18$˚ selection. Since these two selections are imposed on independent data parameters, we realize a greater improvement by using them together. The results of fitting the ToF spectrum for the P15VSGP data in the 4.2–6 and 6–9 MeV bin with $\phi \geq 18$˚ selection and the 2gToF model are shown in figures VI.C.4 and VI.C.5.

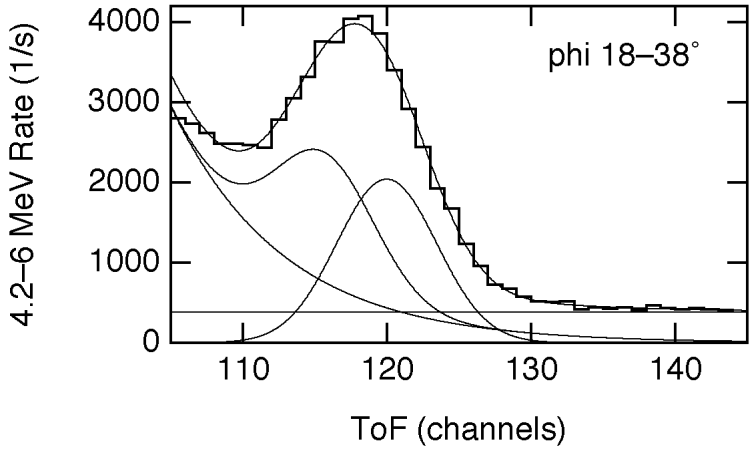

Figure VI.C.4 The 2gToF model ToF fit for $\phi \geq 18$˚ in 4.2–6 MeV P15VSGP data.

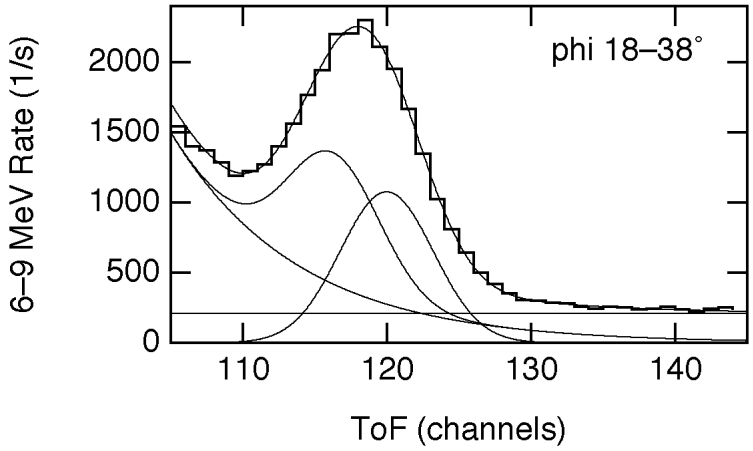

Figure VI.C.5 The 2gToF model ToF fit for $\phi \geq 18$˚ in 6–9 MeV P15VSGP data.

VI.C.3 The VGC Modulation

The modulation factor (M_v) and the signal-to-background ratio (S/B) have been computed for the 4 different data selections, namely 1gToF, 2gToF, 1gToF+ϕ>18˚ and 2gToF+ϕ>18˚. The results for the Virgo and SGP data appear separately in tables VI.C.2 and VI.C.3, respectively. In the Virgo data, with the 2gToF+ϕ>18˚ selection M_v decreases from 3.22 to 2.73 and S/B increases from <0 to 22% for the 4.2–6 MeV bin. M_v decreases from 2.90 to 2.57 and S/B increases from 1.5% to 20% for the 6–9 MeV bin. Smaller improvements are also seen for the SGP data, where the S/B is ~14% and ~12% for the 4.2–6 and 6–9 MeV bins with the 2gToF+ϕ>18˚ selection. The effect of the four selections is shown in figures VI.C.6 and VI.C.7. The ToF-peak rate decreases monotonically with the 1gToF, 2gToF, 1gToF+ϕ>18˚ and 2gToF+ϕ>18˚ selections. We choose the 2gToF+ϕ>18˚ selection to be the optimized-CDG selections in the 4.2 to 9 MeV energy range.

Table VI.C.2 The M_v and S/B ratios in the Virgo data between 4.2 and 9 MeV.

Energy	Event rate (counts/s)			Modu-	S/B
(MeV)	veto2: 0 (CGD)	veto2: 650–800	veto2: 2000–2500	(M_v)	(%)
4.2–6 Virgo					
1gToF	-0.00266	0.0218	0.0700	3.22	<0
1gToF p>18	-0.000072	0.00536	0.0160	2.98	<0
2gToF	0.00126	0.0116	0.0322	2.76	10.8
2gToF p>18	0.000638	0.00293	0.00802	2.73	21.8
6–9 Virgo					
1gToF	0.000174	0.0122	0.0354	2.90	1.43
1gToF p>18	0.000168	0.00252	0.00753	2.99	6.67
2gToF	0.00160	0.00682	0.0170	2.49	23.5
2gToF p>18	0.000392	0.00149	0.00383	2.57	26.3

Table VI.C.3 The M_v and S/B ratios in the SGP data between 4.2 and 9 MeV.

Energy	Event rate (counts/s)			Modu-	S/B
(MeV)	veto2: 0 (CGD)	veto2: 650–800	veto2: 2000–2500	(M_v)	(%)
4.2–6 SGP					
1gToF	-0.00296	0.0212	0.0664	3.13	<0
1gToF p>18	-0.000528	0.00461	0.0154	3.34	<0
2gToF	-0.000869	0.0121	0.0339	2.81	<0
2gToF p>18	0.000425	0.00308	0.00811	2.63	13.8
6–9 SGP					
1gToF	-0.00141	0.0118	0.0345	2.93	<0
1gToF p>18	-0.000130	0.00307	0.00808	2.63	<0
2gToF	-0.000397	0.00650	0.0185	2.84	<0
2gToF p>18	0.000186	0.00162	0.00378	2.34	11.5

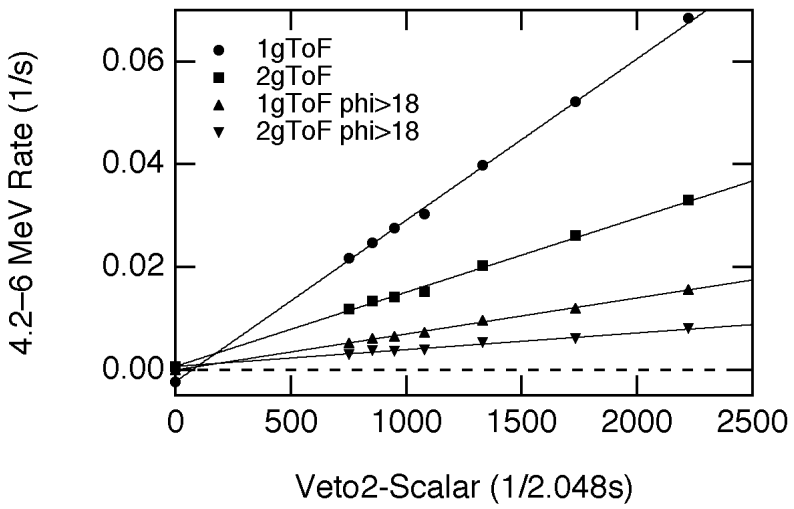

Figure VI.C.6 The 4.2–6 MeV VGCs for the four different ToF-peak rate calculations as described in the text, using P15VSGP data.

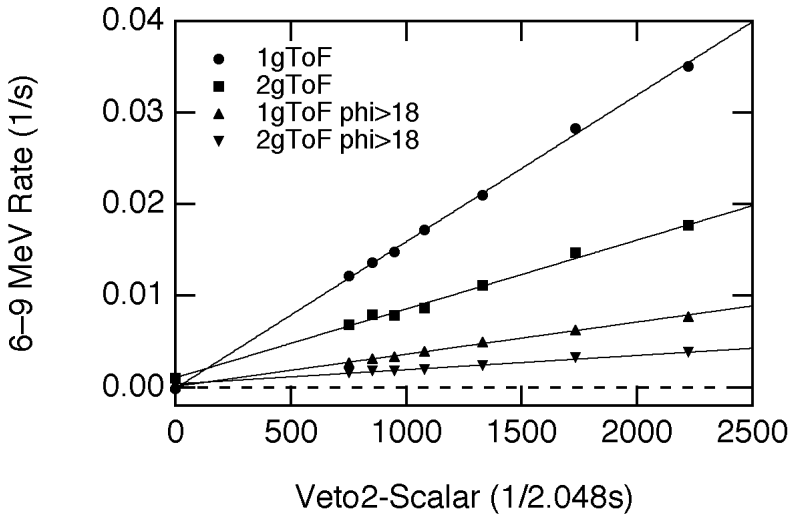

Figure VI.C.7 The 6–9 MeV VGCs for the four different ToF-peak rate calculations as described in the text, using P15VSGP data.

VI.C.4 The 4.2–9 MeV CDG Flux Calculation

The CDG flux has been derived using a linear extrapolation of the ToF-peak VGC with optimized-CDG selections (2gToF+ϕ>18˚) in the 4.2–6 and 6–9 MeV ranges. The VGCs for the Virgo and SGP data in the 4.2–6 and 6–9 MeV bins are plotted in figures VI.C.8 and VI.C.9, respectively. The corresponding CDG flux for the Virgo, SGP and sum datasets are listed in table VI.C.4.

The rates from the Virgo and SGP data are self-consistent for both energy bins. For the Virgo data, the CDG flux is detected with a significance of 2.3 and 2.0 σ in the 4.2–6 and 6–

9 MeV bins, respectively. For the SGP data the significances are 1.2 and 0.6 σ in the 4.2–6 and 6–9 MeV bins, respectively. By summing the Virgo and SGP data the CDG detection significance rises to 2.83 and 2.15 σ in the 4.2–6 and 6–9 MeV bins, respectively.

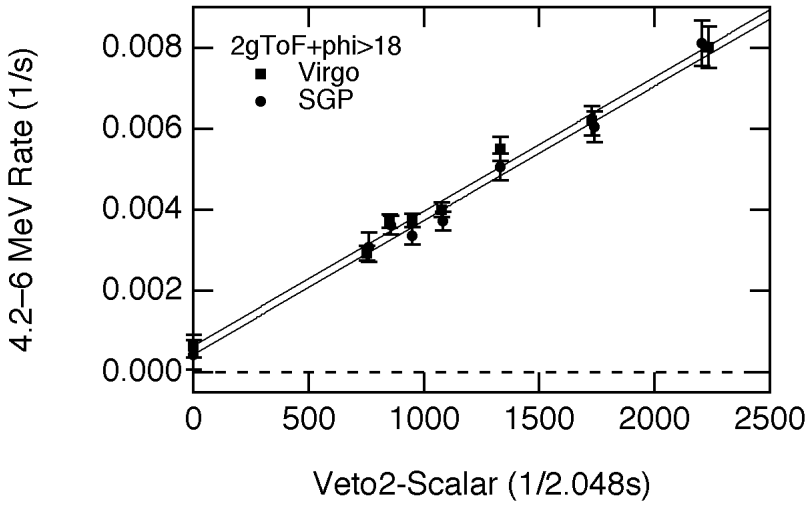

Figure VI.C.8 The 4.2–6 MeV VGC with optimized CDG selections (2gToF+ϕ>18˚) for the Virgo and SGP observations.

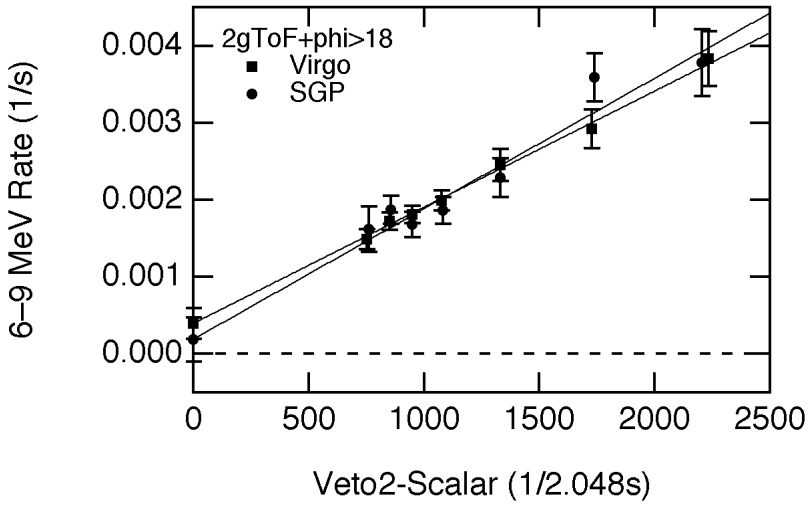

Figure VI.C.9 The 6–9 MeV VGC with optimized CDG selections (2gToF+ϕ>18˚) for the Virgo and SGP observations.

Table VI.C.4 The CDG flux between 4.2 and 9 MeV using 2gToF+ϕ>18˚ selection († 2σ upper-limit).

Data	CDG count rate $\times 10^{-4}$ (counts/s)	Area-Eff (cm^2-sr)	CDG Flux $\times 10^{-5}$ (1/cm^2-s-sr-MeV)
Virgo			
4.2–6	6.4 ± 2.8	5.07	7.0 ± 3.0
6–9	3.9 ± 2.0	4.12	3.2 ± 1.6
SGP			
4.2–6	4.3 ± 3.7	4.95	4.8 ± 4.2
6–9	1.9 ± 2.9	4.06	6.3†
V&SGP			
4.2–6	6.2 ± 2.2	5.03	6.9 ± 2.4
6–9	3.5 ± 1.6	4.10	2.9 ± 1.3

VI.C.5 Consistency Check for the Analysis Method

A consistency check for the CDG analysis method in the 4.2 to 9 MeV range is to compare the CDG flux for subsets of the data (similar to the check in the 9–30 MeV range). The measured 4.2–9 MeV CDG flux for the five independent datasets together with their average value are shown in table VI.C.5 and plotted in figure VI.C.10. The ToF-peak VGCs for the five data subsets are shown in figure VI.C.11.

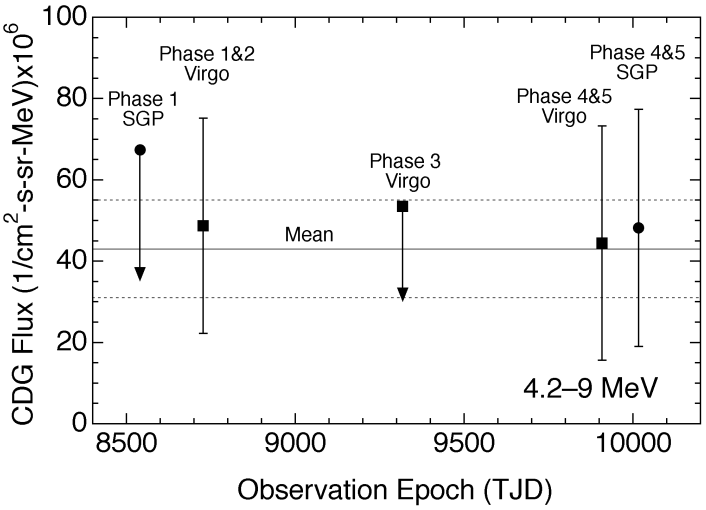

Figure VI.C.10 The measured 4.2–9 MeV CDG flux for the five independent datasets and the average flux together with its 1σ levels.

To test consistency between the measurements, the five independent 4.2–9 MeV measurements were compared to the average value derived from the combined dataset, (4.3 ± 1.2) × 10^{-5} (1/cm^2-s-sr-MeV). The reduced chi-square of the fit is 0.04. The null hypothesis of a constant flux is rejected at only the 5% confidence level. The 4.2–9 MeV flux

measurements are consistent with a constant CDG emission, suggesting that the analysis methods used are robust and reliable.

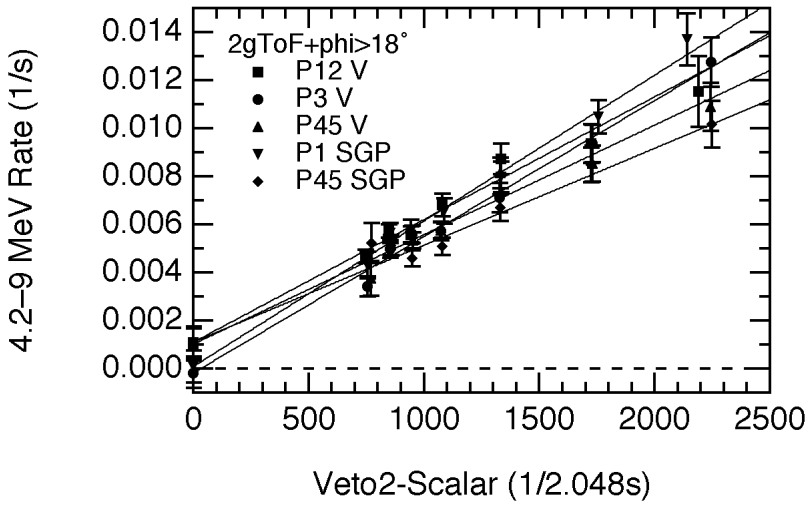

Figure VI.C.11 The 4.2–9 MeV VGC for the five independent datasets.

Table VI.C.5 The total 4.2–9 MeV flux with 2gToF+ϕ>18° selection († 2σ upper-limit).

Data	4.2–9 MeV CGD Rate $\times 10^{-4}$ (counts/s)	Effective-Area (cm^2-sr)	4.2–9 MeV CDG Flux $\times 10^{-5}$ ($1/cm^2$-s-sr-MeV)
Virgo+SGP	9.7 ± 2.7	4.66	4.3 ± 1.2
Virgo	10.6 ± 3.4	4.70	4.7 ± 1.5
SGP	5.6 ± 4.7	4.60	2.5 ± 2.2
P12V	10.9 ± 5.9	4.65	4.9 ± 2.6
P3V	–1.9 ± 6.1	4.72	$5.34^{\dagger}$
P45V	10.1 ± 6.5	4.72	4.4 ± 2.9
P1SGP	0.69 ± 6.8	4.41	$6.74^{\dagger}$
P45SGP	10.9 ± 6.6	4.72	4.8 ± 2.9

VI. D. The 2.7–4.2 MeV CDG Analysis

Below 4.2 MeV is the domain of the long-lived background component. The 2.7–4.2 MeV ToF-peak rates contain events from the long-lived background component in addition to the contributions from the prompt and CDG components. In this energy range, the dominant source of long-lived background is from the decay of the ^{24}Na isotope where the 2.754 photon undergoes energy loss in D2 and the 1.368 photon scatters in D1. There are also two unidentified lines present in the E2 spectrum at ~2.94 and ~2.57 MeV that contribute to the ETOT spectrum in the 2.7–4.2 MeV range. As will be shown, by using

special data selections we can virtually eliminate the contributions of these lines, making their identification less important.

VI.D.1 The ToF Spectrum

As discussed earlier in section V.D, the ^{24}Na events in the telescope data are predominantly type C events showing a ToF-peak around channel 116 due to the geometry of 2-photon type C events. This ToF behavior is seen in the simulations of the ^{24}Na decay and as well as in the data (figure VI.D.1). The lower position of the ^{24}Na ToF-peak suggests that a two-gaussian ToF model (2gToF) should be used (as in the 4.2–9 MeV CDG analysis) to determine the ^{24}Na events simply from the ToF fits. However, the scenario is not quite as simple. To understand this, we must realize that the ToF resolution is degrading with energy (see section V.A). The width of the single gaussian ToF (1gToF) peak between 3 and 4 MeV is ~4.5 channels making it difficult to separate the two ToF peaks at 116 and at 120. Secondly, the lower ToF peak at ~116 channel is intense, since both prompt and long-lived events contribute to it. Therefore, one requires an accurate description of the ToF spectrum to be able to correctly separate the two components. However, the background in the 2.7–4.2 MeV region show an energy spectrum signature that can be exploited to estimate its intensity. This differs from the 4.2–9 MeV range where there are no spectral features for the lower ToF peak at channel 116.

In the light of these points, the approach in the 2.7–4.2 MeV energy range (and also for the lower energy intervals) is to first determine the ToF-peak rates using the one gaussian model that includes the contribution from the ^{24}Na component. We then fit the characteristic decay lines in the individual detector spectrum to calculate and eventually subtract the ^{24}Na and other line contributions from the ToF-peak rates. The long-lived background-corrected VGCs are then extrapolated to zero veto rate to compute the CDG count rate.

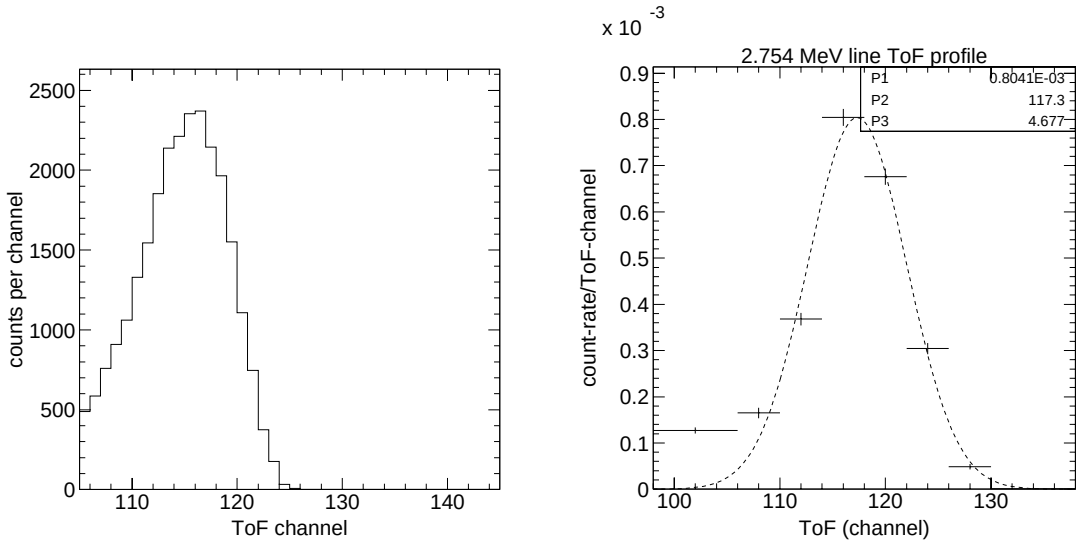

(a) (b)

Figure VI.D.1 (a) The ^{24}Na ToF spectrum from simulations and; (b) The ToF profile of the 2.754 MeV line from ^{24}Na from data.

VI.D.2 Special Data Selections

The data with the lowest SAA dosage

The time-averaged prompt activity is roughly constant over the 5 years of observations, however this is not the case for the long-lived background components (section V.B). Observations when the intrinsic ^{24}Na activity is low are best for studying the 2.7–4.2 CDG flux due to the higher S/B ratio. The observations used for the 2.7–4.2 MeV CDG measurement are those for all the Phase 2 Virgo observations and for all the Phase 3 Virgo observations prior to the reboost, labeled as the "P23a" dataset. The reason for choosing these observations is that their spacecraft altitude is the lowest and hence the SAA dose is a minimum.

The E1 950–1250 keV selection to enhance the 2.754 line in E2

The ^{24}Na decays with photon energies of 2.754 and 1.368 MeV. The standard-CDG data selections eliminate most events where the 1.368 photon interacts in D2 and the 2.754 photon interact in D1 (explained in section V.C). Therefore the problematic ^{24}Na events are the converse, i.e., the 2.754 photons interact in D2 and 1.368 photons trigger D1. As a result, a narrow selection in D1 energy around the Compton-edge of the 1.368 photon will enhance the 2.754 line in E2 with respect to the continuum. The Compton edge for a 1.368 MeV

photon in D1 is 1.153 MeV. All thin, low Z scintillators have the maximum energy deposit at the Compton-edge energy since the photopeak efficiency is very low. An E1 energy cut of 950–1250 keV, labeled as the "24Na-E1" cut, will favor the 1.368 MeV photon Compton edge in D1. This cut increases the 2.754 MeV line-to-continuum ratio as seen in the E2 energy spectrum in figure VI.D.2.

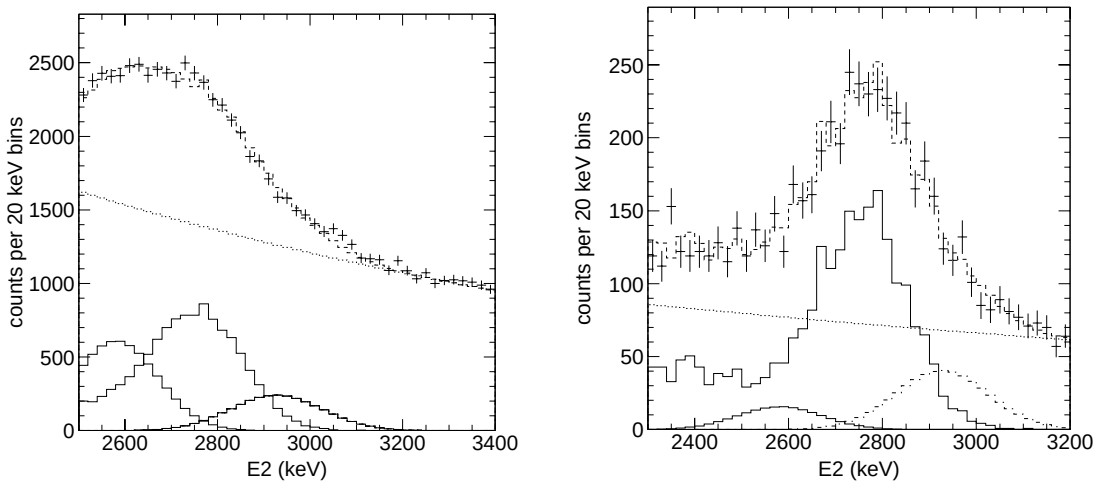

Figure VI.D.2 The P23a E2 spectrum about the 2.754 MeV line from ^{24}Na decay for (a) standard CDG selections and, (b) 24Na-E1 selections (E1 950–1250 keV); including the fit components of the ^{24}Na-template, an exponential and two gaussians at 2.58 and 2.94 MeV.

Such an E2 spectrum with E1 950–1250 keV is used to calculate the ^{24}Na intensity as a function of veto rate. Once we determine the ^{24}Na intensity (and its VGC) for this selection, the ^{24}Na response from simulations can be used to correctly scale the measured intensity to any other data selection. The ability to scale the long-lived background line intensities to any other data selection is the advantage of having a simulated isotope-decay response.

The 2.754 MeV line region in E2 with the 24Na-E1 selections (and a ToF 110–130 channels cut) is fit for the summed veto-bins P23a data and is plotted in figure VI.D.2. The fit includes two gaussians for the 2.58 and 2.94 MeV photopeaks, an exponential for the continuum and the template for the ^{24}Na response (2.754 MeV line and its tail). The fits are performed as a function of veto rate. The ^{24}Na VGC scaled to the 2.7–4.2 MeV bin in ETOT is shown in figure VI.D.3. The ^{24}Na VGC shows no non-linearity at low veto rates as seen in

the P2345 data (see section V.E), but is consistent with a constant ^{24}Na rate (the data point in the veto2: 0–650 bin is the average rate).

For comparison the ^{24}Na VGC from fits to the E2 spectrum with standard-CDG selection, i.e., an open E1 window is shown in figure VI.D.2. The corresponding VGC for the 2.7–4.2 MeV bin in ETOT is also plotted in figure VI.D.3. Within uncertainties the two ^{24}Na VGCs show similar behavior. An advantage of fitting the lines for the standard-CDG data selections (i.e., open ϕ selections) is that we now also have the VGCs for the 2.58 and 2.94 MeV lines (figure VI.D.4). The 2.58 and 2.94 MeV line VGCs can be used to correct for their contribution to the 2.7–4.2 MeV VGCs. However the average ^{24}Na rate using standard-CDG selection is ~27% higher than the ^{24}Na rate using the 24Na-E1 cut. Considering the large increase in S/B for the 2.754 MeV line with the ^{24}Na-E1 cut, its results for the ^{24}Na rate are more reliable. The 27% change could be considered a rough measure of the systematic uncertainties in the method to calculate the ^{24}Na intensity.

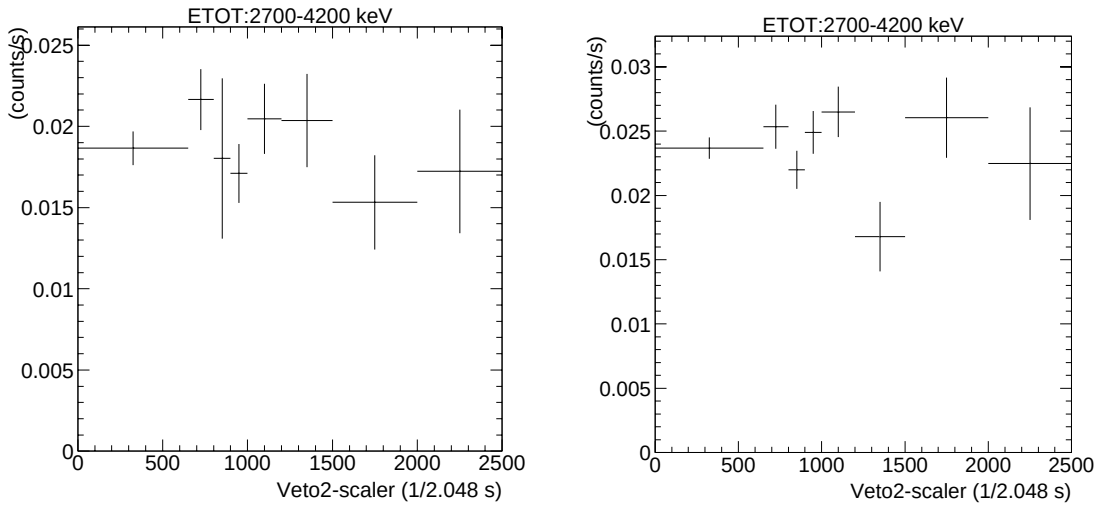

(a) (b)

Figure VI.D.3 The ^{24}Na VGC for P23a 2.7-4.2 MeV (a) using 24Na-E1 selections (E1: 950–1250 keV) and, (b) using standard-CDG selections (E1: 70–20000 keV). The data point in the veto2: 0–650 bin is the average rate.

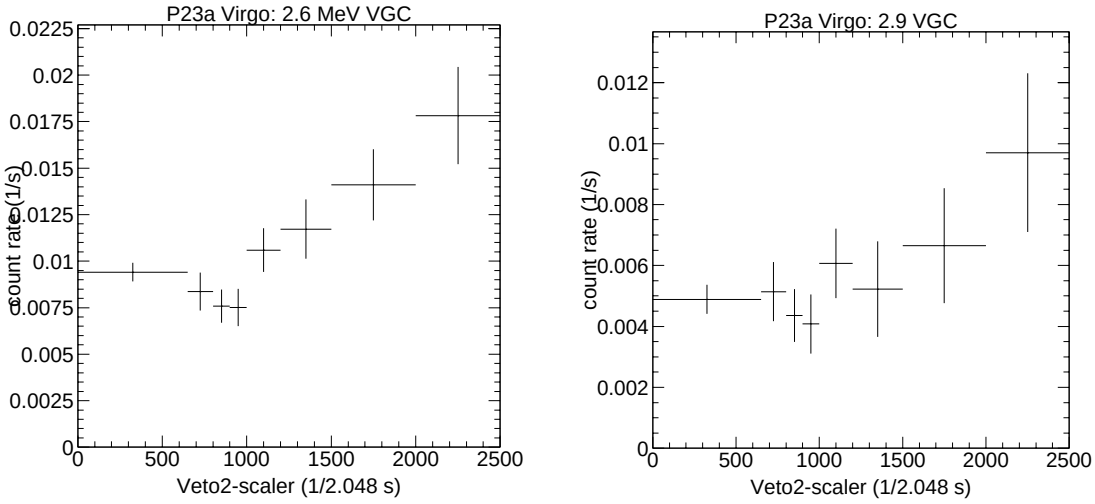

(a) (b)

Figure VI.D.4 The (a) 2.6 MeV and (b) the 3.0 MeV VGC for 2.7-4.2 MeV using P23a data with standard-CDG selections. The data point in the veto2: 0–650 bin is the average rate.

The ϕ 22–38˚ selection to suppress ^{24}Na events

With a reliable method to estimate the ^{24}Na intensity and its veto rate dependence in the 2.7–4.2 MeV range or any other data selection, the next step is to compute the ToF-peak VGC in the 2.7–4.2 MeV bin for the P23a data.

The ^{24}Na component together with the 2.6 and 2.9 MeV lines are substantially suppressed with the ϕ >22˚ selection. This was discussed in section V.C. The disappearance of the 2.754 MeV photopeak region including the 2.6 and 2.9 MeV peaks in E2 by the ϕ 22–38˚ selection was clearly seen in figure V.C.22. Figure V.C.24 showed the distribution of ETOT 2.7–4.2 MeV events to the E2 spectrum. The contributions from the ^{24}Na component together with the 2.6 and 2.9 MeV lines to ETOT 2.7–4.2 MeV were minimized with the ϕ>22˚ selection.

The 2.7–4.2 MeV VGC for all three ToF components with their respective straight line fits for the ϕ >22˚ data selection and standard-CDG data selections are plotted in figure VI.D.5. Note the large difference (about a factor of 10) in count rates between the two selections.

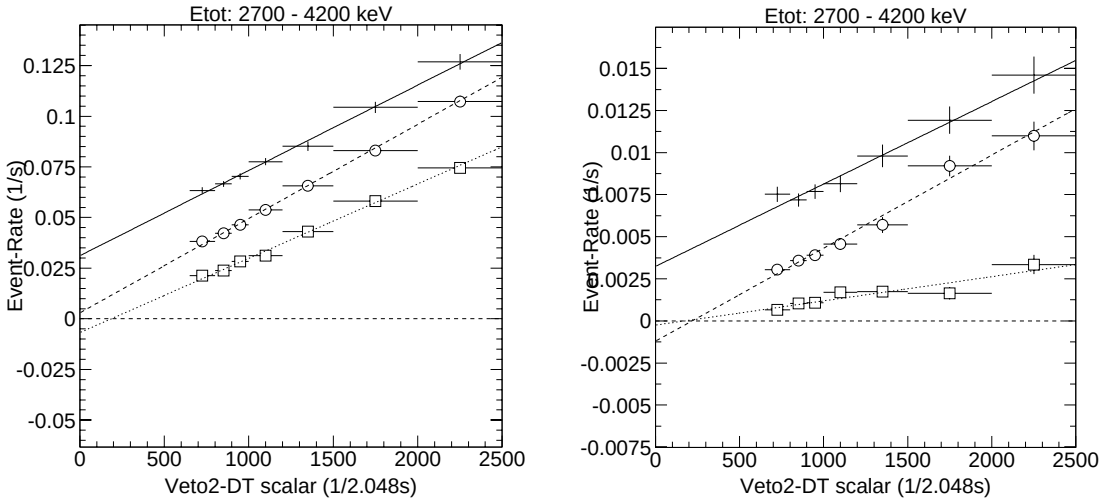

(a) (b)

Figure VI.D.5 The P23a 2.7–4.2 MeV VGC for all three ToF components with their respective straight line fits (a) using standard CDG-selections (ϕ 6–38˚); and (b) using ϕ 22–38˚ selection (+: gaussian; square: constant; circle: exponential).

The 2.58 and 2.94 MeV lines are two-photon events, as seen by the presence of photopeaks in the E2 spectrum. The ETOT 2.7–4.2 MeV counts with ϕ>22˚ selection accept only events with E2 energy deposits less than ~2600 keV, therefore the 2.9 MeV line makes no contribution to the 2.7–4.2 MeV counts in ETOT region with a ϕ>22˚ restriction. With the ϕ>22˚ selection, a minimum E1 energy deposit of ~1.5 MeV is required with the 2.58 MeV line in D2 to register telescope events, from the Compton-scattering formula (see figure VI.D.6). Incidentally, the 2.6 line counts are lower for the E1:950–1250 keV selection (see figure VI.D.2) indicating that the second photon associated with the 2.6 MeV peak is most likely below 1000 keV in the E1 spectrum. As a result the 2.6 MeV gaussian events with ϕ>22˚ does not contribute to the 2.7–4.2 MeV bin in ETOT. The 2.6 MeV line seems to be prompt in nature (see section V.E) and will be subtracted in the VGC extrapolation. To summarize, the 2.6 and 2.9 MeV lines do not contribute to the ETOT 2.7–4.2 MeV bin with the ϕ>22˚ selection.

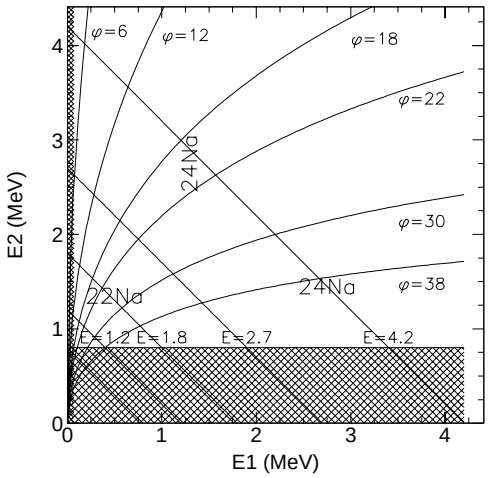

Figure VI.D.6 The E1–E2 parameter space with lines of constant ETOT and constant ϕ. The dominant position of ^{24}Na and ^{22}Na events are marked.

With the ϕ 22–38˚ selection, the ^{24}Na count rate decreases by a factor of ~12 while the instrument effective-area for the CDG radiation only decreases by a factor of ~4. This demonstrates that the ϕ 22-38˚ selection is effective in enhancing the CDG radiation relative to the ^{24}Na component. Henceforth, the ϕ 22–38˚ selection is the optimized-CDG data selection in the 2.7–4.2 MeV range.

The E2 ToF-cut corrections

The ToF-peak VGCs are computed using the total gaussian counts for the fitted ToF peak. To produce the E2 count spectra we apply a 110–130 ToF selection to select on the forward peak so as to compute the ^{24}Na count within the forward peak, therefore, parts of the ^{24}Na gaussian tail are cut by the ToF selection. Although most of the ToF peak events within 110–130 ToF are assigned to the ToF-peak in the 1gToF fit, nevertheless, there are ^{24}Na events outside the 110–130 ToF cut region that contribute to the ToF-peak gaussian counts and vise-versa. We should therefore apply a correction to properly scale the ^{24}Na counts determined from the ToF 110–130 region into the counts in the ToF-peak VGCs.

The differences in line intensities from the ToF cut region to the ToF-peak fits cannot be exactly determined because we do not know the true distribution of the ^{24}Na events (or the lines) in the ToF spectrum. Nevertheless, an estimate of the fraction of ^{24}Na events lost due to the cut can be determined by investigating the ToF distribution of the 2.754 MeV in E2 (see

figure VI.D.1(b)). The fit of a gaussian to the 2.754 MeV ToF distribution results in a ToF-peak position of 117.3 and a width of 4.7 channels. The 110–130 ToF cut corresponds to integrating the gaussian from –1.57 to 2.71 σ. This corresponds to 93.8% of the gaussian area within the 110–130 ToF range, hence the ToF-corrections to properly scale the 110–130 counts is 1.07. Therefore, we scale the ^{24}Na (and the 2.6 and 3.0) activity by 1.07 before subtracting them from the ToF-peak VGCs. Considering the much greater uncertainties in the ^{24}Na activity (~25%) and the extrapolated rates (~50%), this ToF-correction (~7%) is small.

VI.D.3 The 2.7–4.2 MeV CDG Flux Calculation

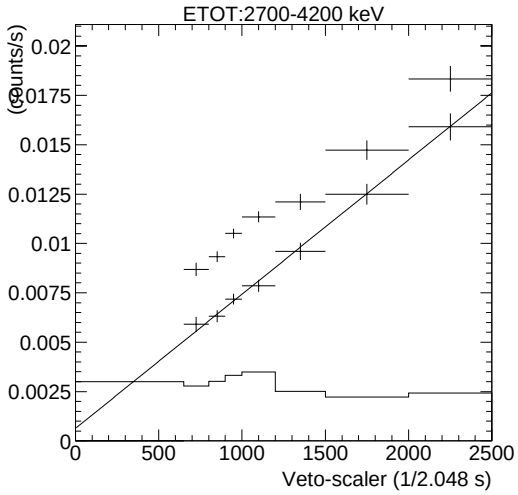

Figure VI.D.7 The P23a ^{24}Na corrected 2.7–4.2 MeV VGC for ϕ 22–38˚ used to compute the 2.7–4.2 MeV CDG flux.

The method for determining the 2.7–4.2 MeV CDG measurement is as follows: First compute the 2.7–4.2 MeV ToF-peak VGC for ϕ 22–38˚ using the P23a data, then determine the ^{24}Na intensity as a function of veto bin using the E1 950–1250 keV selection. Scale the ^{24}Na VGC from the E1: 950–1250 keV dataspace to the ϕ≥22˚ ETOT 2.7–4.2 MeV dataspace. Subtract the scaled ^{24}Na VGC from the 2.7–4.2 MeV ToF-peak VGC. The residual counts now consist of only the prompt background and the CDG events. As argued earlier the contributions from the 2.9 line in the ϕ≥22˚, 2.7–4.2 MeV data can be assumed to be zero. The 2.6 MeV line although prompt is also suppressed ϕ≥22˚ and is accounted for in the extrapolation. The extrapolated rate at zero veto-scaler rate is a reliable measure of the CDG count rate in the 2.7–4.2 MeV bin. The P23a ^{24}Na subtracted 2.7–4.2 MeV VGC for ϕ 22–

38˚ is shown in figure VI.D.7 and the results are presented in table VI.D.1. The table also includes the relative contributions of the ^{24}Na, prompt and CDG components to the count rate for veto2 rate bin 650–800 (Rate@v2:650). The 2.7–4.2 MeV CDG S/B ratio is ~19% and the VGC modulation factor, M_v is ~2.32. The 2.7–4.2 MeV CDG flux is measured with a statistical significance of 1.99σ and has a value of $(2.45 \pm 1.23) \times 10^{-4}$ photons/cm^2-s-sr-MeV.

Table VI.D.1 The results for 2.7–4.2 MeV CDG analysis for P23a data and ϕ 22–38˚ with the ^{24}Na activity determined using 24Na-E1 selections.

Rates —		
average ToF-peak rate	(1/s)	0.00866 ± 0.00030
ToF-peak rate in v2:650–800	(1/s)	0.00752 ± 0.00045
average ^{24}Na rate	(1/s)	0.00174 ± 0.00010
Ratios —		
^{24}Na rate /Rate@v2:650	(%)	23.2
Prompt rate/Rate@v2:650	(%)	59.7
M_v for ToF-peak VGC		1.94
(ToF-peak – ^{24}Na) VGC —		
VGC M_v		2.36
VGC slope	(1/s-veto2)	$(5.09 \pm 0.58) \times 10^{-6}$
S/B: CDG rate/ Rate@v2:650	(%)	17.1
CDG (constant) rate	(1/s)	0.00129 ± 0.00065
Effective-Area	(cm^2-sr)	3.50
CDG flux	(1/cm^2-s-sr-MeV)	$(2.45 \pm 1.23) \times 10^{-4}$

VI.D.4 Consistency Check for the Analysis Method

We perform two consistency checks for the 2.7–4.2 MeV CDG flux result.

(1) Test the sensitivity of the CDG rate to the exact shape of the ^{24}Na VGC.

The ^{24}Na VGC typically show non-linearity at low veto-scaler rates when data with different activation (SAA dosage) is added, as discussed in section V.E. Recall that we use P23a data that has the lowest (and similar) SAA dosage. The P23a ^{24}Na VGC do not show any non-linearities at low veto rates.

Extrapolate the P23a ϕ≥22˚ ToF-peak VGC before correcting for the ^{24}Na rates, then subtract the veto-averaged ^{24}Na rate from this extrapolated rate to estimate the CDG count rate. We have switched the order of the prompt and long-lived corrections, however the resulting CDG intensities from either subtracting ^{24}Na before or after extrapolation are consistent with each other. The differences are less than 0.5σ. The CDG intensities from both methods are shown in table VI.D.2.

Table VI.D.2 The 2.7–4.2 MeV CDG rates for subtracting the ^{24}Na intensity before and after extrapolating the ToF-peak VGC (ϕ 22–38˚ and P23a data).

Extrapolation method	Rate (1/s)	Flux $\times 10^{-4}$ (1/cm^2-s-sr-MeV)
average 24Na rate	0.00174 ± 0.00010	
CDG: ToF-peak VGC	0.00323 ± 0.00065	
CDG: ToF-peak VGC – average 24Na	0.00149 ± 0.00066	2.84 ± 1.26
CDG: (ToF-peak – 24Na) VGC	0.00142 ± 0.00065	2.45 ± 1.23

(2) Compute the CDG rate for standard CDG selections (ϕ 6–38˚).

Start with the P23a 2.7–4.2 MeV ToF-peak VGC for standard CDG selections (ϕ 6–38˚) which contain contributions from the 2.6 and 2.9 MeV lines. As before calculate the ^{24}Na VGC with E1: 950–1250 keV selection and scale it to the ϕ 6–38˚ ETOT 2.7–4.2 MeV selection.

The E1 threshold is set at 70 keV, therefore all events above 2630 keV in E2 will have energies greater than 2700 keV in ETOT. The 2.94 MeV peak 1σ energy resolution is 99 keV. The low energy limit for the 2.93 MeV gaussian (position minus 3σ resolution) corresponds to ~2620 keV in E2, therefore the entire 2.93 MeV peak counts are contained in the 2.7–4.2 MeV bin in ETOT. We can therefore subtract the 2.94 MeV gaussian VGC from the 2.7–4.2 MeV VGC with standard-CDG selections. From the above argument, all counts from the 2.6 MeV peak above 2630 keV will also reside in the 2.7–4.2 MeV bin in ETOT. The events above 2630 keV correspond to 29.11% of the total 2.6 MeV peak counts. We can scale the 2.6 MeV VGC by 29.11% to estimate its contribution to the 2.7–4.2 MeV bin in ETOT.

The VGCs used for extrapolation to determine the CDG count rate using standard CDG selections are computed for three separate methods and the results are tabulated below: (1) Correct only for the ^{24}Na VGC prior to extrapolation — this serves as an upper limit to the CDG flux since the contribution from the 2.9 and 2.6 MeV lines are not yet subtracted; (2) Correct for the ^{24}Na, 2.9 MeV and scaled 2.6 MeV line VGCs prior to extrapolation — this would be the correct approach if the origin and contributions of each the 2.9 and 2.6 MeV line components to the 2.7–4.2 MeV were unambiguously known; (3) Correct for the ^{24}Na and 2.9 MeV VGC prior to extrapolation — the 2.9 MeV is probably long-lived hence

subtracted while the 2.6 MeV line is probably prompt and hence accounted for in the VGC extrapolation.

The results of VGC extrapolation for the three separate methods are shown in table VI.D.3. The 2.7–4.2 MeV VGC using standard-CDG selections with ^{24}Na and 3.0 MeV line subtracted and with ^{24}Na, 3.0 and 2.6 MeV line subtracted are potted in figure VI.D.8. The CDG flux for ϕ 6–38˚selection in all three extrapolation cases are consistent with the results using ϕ 22–38˚ selections demonstrating that we are able to correctly account for the 2.6 and 3.0 MeV contributions in the data. It is encouraging to get consistent CDG fluxes when using data selections (ϕ 6–38˚) where the average background rate is about ten times higher than for the optimized CDG data selections (ϕ 22–38˚).

Table VI.D.3 The results for 2.7–4.2 MeV CDG analysis for P23a data and ϕ 6–38˚

Effective-Area	(cm^2-sr)	14.25
Rates —		
average ToF-peak rate	(1/s)	0.07789 ± 0.00105
ToF-peak rate in v2:650–800	(1/s)	0.06344 ± 0.00156
average ^{24}Na rate	(1/s)	0.01866 ± 0.00104
average 3.0 MeV rate	(1/s)	0.004919 ± 0.000413
average 2.6 MeV rate	(1/s)	0.002670 ± 0.000134
CDG flux for ϕ 6–38˚		
(ToF-peak–^{24}Na) VGC	(1/cm^2-s-sr-MeV)	0.000349 ± 0.000177
(ToF-peak–^{24}Na–3.0) VGC	(1/cm^2-s-sr-MeV)	0.000238 ± 0.000326
(ToF-peak–^{24}Na–3.0–2.6) VGC	(1/cm^2-s-sr-MeV)	0.000203 ± 0.000204
CDG flux for ϕ 22–38˚		
CDG: (ToF-peak–^{24}Na) VGC	(1/cm^2-s-sr-MeV)	0.000245 ± 0.000123

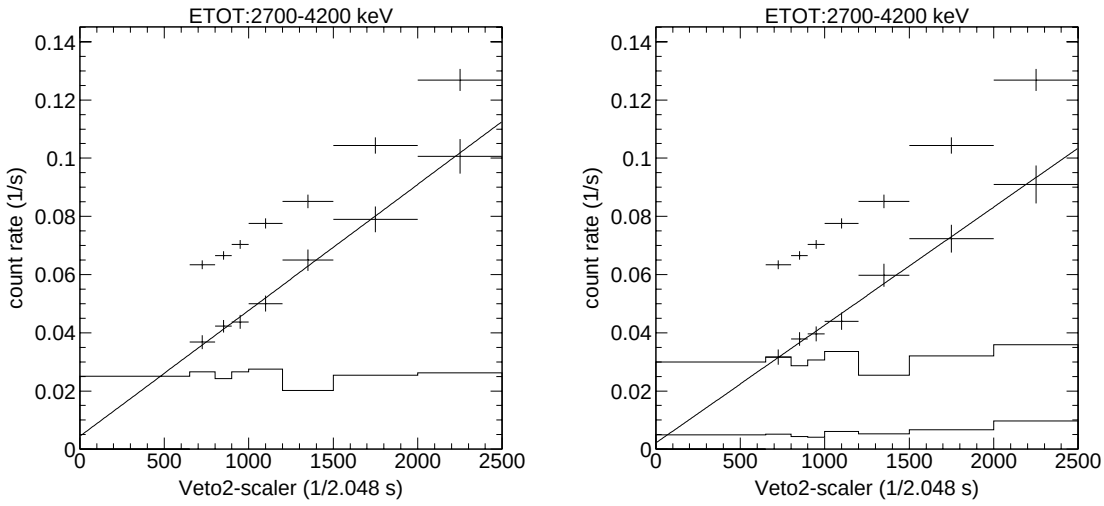

(a) (b)

Figure VI.D.8 The 2.7–4.2 MeV VGC for ϕ 6–38˚ with (a) ^{24}Na and 3.0 MeV line subtracted; and (b) with ^{24}Na, 3.0 and 2.6 MeV line VGCs subtracted prior to extrapolation.

VI. E. The 1.8–2.7 MeV CDG Analysis

For the 1.8–2.7 MeV range, the analysis is similar to that for the 2.7–4.2 MeV energy range. We first determine the ToF-peak rates using the one gaussian ToF model that includes the contribution from line components within the ToF-peak rates. We then fit the characteristic decay lines in the individual detector spectrum to calculate and eventually subtract their contributions to the ToF-peak rates. The long-lived background corrected ToF-peak VGCs are then extrapolated to zero veto rate to determine the CDG count rate. The ETOT 1.8–2.7 MeV counts consist of the 2.2 MeV and ^{28}Al events together with the contributions from the prompt and CDG components. In the E2 spectrum, the 2.2 MeV photon produces a continuum below ~2200 keV and the signature of the ^{28}Al decay is the 1.8 MeV photopeak. Since the 2.2 MeV is a prompt background source, its contributions are automatically corrected during the veto rate extrapolation. For a detailed description of the 2.2 MeV VGC see section V.E.

VI. E. 1 The E2 Spectral Fit

To minimize the background intensity, the P23a data are again used for the 1.8–2.7 MeV CDG analysis. The ϕ 22–38˚ selection suppresses the ^{24}Na component and the 2.6 and 3.0 line

contributions (see section V.C). The ETOT 1.8–2.7 MeV and ϕ 22–38˚ cuts select events with energy only less than ~1900 keV in E2. Therefore the 2000–2400 keV excess in the E2 spectrum is also significantly reduced (see section V.C).

In figure VI.E.1(a) the P23a E2 spectrum is plotted together with the exponential function representing the continuum background. Figure VI.E.1(b) shows the exponential subtracted E2 spectrum that represents the line emissions. There are no special selections applied to optimize for the ^{28}Al line in the E2 spectrum. As described in section V.C, after subtracting the ^{24}Na and 2.2 MeV contributions, the 1.8 MeV photopeak for ^{28}Al is fit in the narrow E2 range 1600–1900 keV, superimposed over a flat continuum. The continuum-subtracted E2 spectrum with the fitted ^{24}Na, 2.6 and 3.0 gaussians, 2.2 MeV and ^{28}Al components is shown in figure VI.E.2.

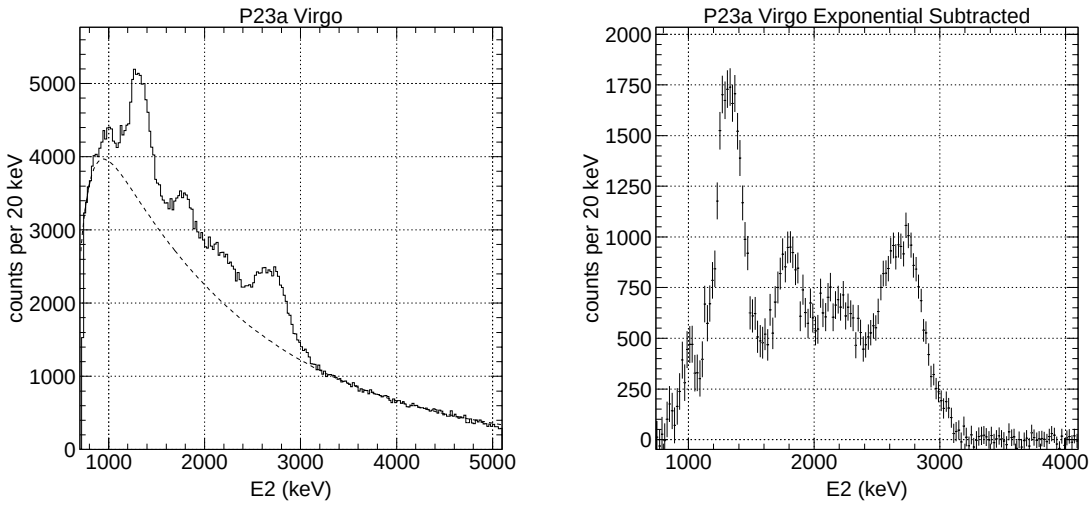

(a) (b)

Figure VI.E.1 (a) The P23a E2 spectrum together with the exponential continuum function; and (b) the E2 spectrum with the exponential-continuum subtracted to determine the component from the lines.

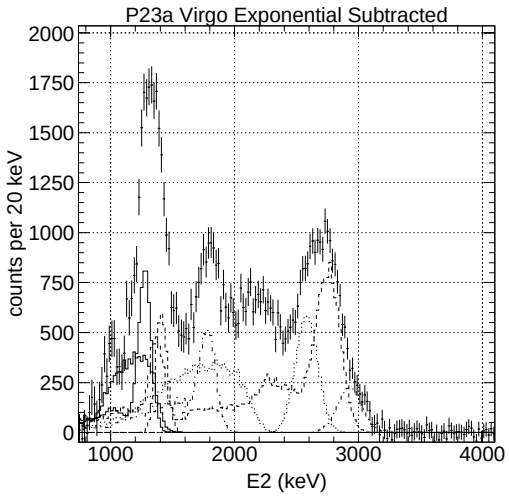

Figure VI.E.2 The continuum-subtracted E2 spectrum with the ^{24}Na, 2.6 and 3.0 gaussians, 2.2 MeV and ^{28}Al components.

The ^{28}Al VGC

The ^{28}Al intensity is determined as a function of veto-scaler to produce the ^{28}Al VGC. Once we determine the ^{28}Al intensity, its response for a different data selection can be determined from the ^{28}Al simulations. I have plotted the ^{28}Al VGC for the 1.8–2.7 MeV $\phi \geq 22^{\circ}$ selection in figure VI.E.3. It shows a linear dependence with veto rate indicative of its relatively prompt nature ($\tau_{1/2} \approx 2.25$ min.).

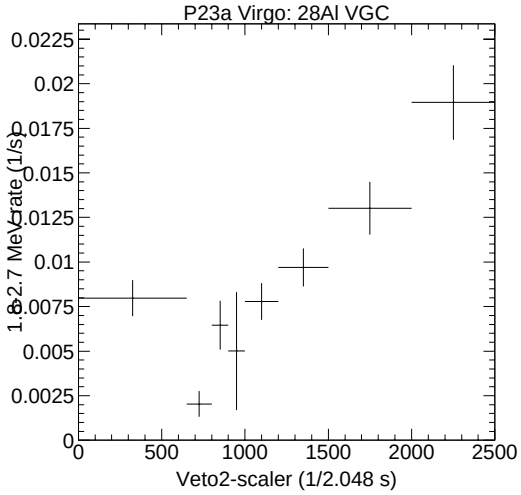

Figure VI.E.3 The ^{28}Al VGC in ETOT 1.8–2.7 MeV for the P23a data. The average rate is plotted in the v2: 0–650 bin.

The E2 ToF-cut corrections

Similar to the 2.7–4.2 MeV work, a ToF correction is applied to properly scale the fitted line intensities determined from the ToF 110–130 region to the counts in the ToF-peak VGCs. The correction factor is determined from the 1gToF fit to the ToF-peak in ETOT. The ToF-exponential model results in ToF-peak position at 119.3 with a width of 4.9 channels, corresponding to a correction of 1.05. This correction is applied to the line intensities before subtracting their contribution from the ToF-peak VGCs.

VI.E.2 The 1.8–2.7 MeV CDG Flux Calculation

The 1.8–2.7 MeV CDG flux measurement begins by calculating the ToF-peak VGC for ϕ 22–38˚ using the P23a data. The ^{24}Na, 2.2 MeV and ^{28}Al VGCs are determined as described earlier. The isotope intensities are scaled to the $\phi \geq 22^{\circ}$ ETOT 1.8–2.7 MeV dataspace.

The ^{28}Al and the 2.2 MeV lines are both prompt in nature and not subtracted explicitly. The 2000–2400 keV residuals and tail from the 2.6 MeV line is minimized by the ϕ 22–38˚ selection, but they also appear to be prompt in nature. The scaled ^{24}Na VGCs are subtracted from the 1.8–2.7 MeV ToF-peak VGC. The residual VGC counts consist of the prompt and the CDG events. Hence, the ^{24}Na-subtracted VGC extrapolated to zero veto-rate is a reliable measure of the CDG count rate in 1.8–2.7 MeV range.

The ^{24}Na subtracted 1.8–2.7 MeV VGC for P23a ϕ 22–38˚ is shown in figure VI.E.4. The results for VGC extrapolation are presented in table VI.E.1. The table also includes the relative contributions of the ^{24}Na, ^{28}Al, prompt and CDG components to the count rate for veto2-rate bin 650–800 (Rate@v2:650). The 1.8–2.7 MeV CDG S/B ratio is 27% and the VGC modulation factor M_v is 1.97.

The extrapolated rate at zero veto-rate using the ^{24}Na-corrected 1.8–2.7 MeV ToF-peak VGC with $\phi \geq 22^{\circ}$ results in a CDG count rate of 0.0044 ± 0.0010 (1/s). The effective area with the corresponding data selections is 4.04 (cm^2-sr). This gives a flux $(1.21 \pm 0.29) \times 10^{-3}$ photons/cm^2-s-sr-MeV for the 1.8–2.7 MeV CDG radiation. The 1.8–2.7 MeV CDG measurement has a statistical significance of 4.2σ.

Table VI.E.1 The results for 1.8–2.7 MeV CGD analysis using P23a data and ϕ 22–38˚.

Rates —		
average ToF-peak rate	(1/s)	0.0208 ± 0.0004
ToF-peak rate in v2:650–800	(1/s)	0.0160 ± 0.0007
average ^{24}Na rate	(1/s)	0.0025 ± 0.0001
average ^{28}Al rate	(1/s)	0.0026 ± 0.0003
Ratios —		
^{24}Na rate/Rate@v2:650	(%)	14.9
Prompt rate/Rate@v2:650	(%)	49.3
Mv for ToF-peak VGC		2.12
(ToF-peak–^{24}Na) VGC —		
VGC M_v		1.97
VGC slope	(1/s-veto2)	$(1.25 \pm 0.10) \times 10^{-5}$
S/B: CDG rate/ Rate@v2:650	(%)	27.5
CDG (constant) rate	(1/s)	0.0044 ± 0.0010
Effective-Area	(cm^2-sr)	4.04
The 2.7–4.2 MeV CDG flux	($1/cm^2$-s-sr-MeV)	$(1.21 \pm 0.29) \times 10^{-3}$

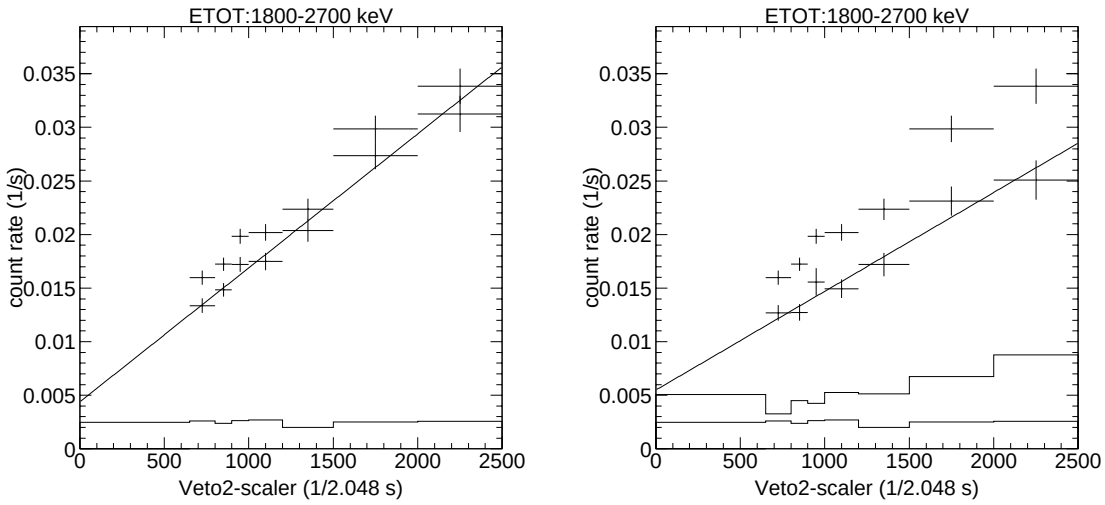

(a) (b)

Figure VI.E.4 The 1.8–2.7 MeV for ϕ 22–38˚ selection with (a) only ^{24}Na subtracted ;and (b) with ^{24}Na+^{28}Al subtracted from the ToF-peak VGCs prior to extrapolation.

VI. E. 3 Consistency Check for the Analysis Method

We perform two consistency checks for the 1.8–2.7 MeV CDG flux results.

(1) Compare the CDG count rate for ^{24}Na-corrected VGC extrapolation to the CDG count rate for ^{24}Na+^{28}Al-corrected VGC.

The resulting CDG intensities from both ^{24}Na-corrected VGC and ^{24}Na+^{28}Al-corrected VGC methods are listed in table VI.E.2. The two CDG count rates are consistent with each other, their differences are less than a 1σ. Subtracting the ^{28}Al VGC prior to VGC

extrapolation does not significantly change the residual CDG count rates, i.e., ^{28}Al events behave like a prompt background component.

Table VI.E.2 The effect of ^{28}Al subtraction to the 1.8–2.7 MeV analysis for P23a data.

CDG Extrapolation method	Rate (1/s)	Flux $\times 10^{-3}$ (1/cm^2-s-sr-MeV)
(ToF-peak–^{24}Na) VGC	0.0044 ± 0.0011	1.21 ± 0.29
(ToF-peak–^{24}Na–^{28}Al) VGC	0.0055 ± 0.0012	1.51 ± 0.32

(2) Compute the CDG rate for standard CDG selections, i.e., for the ϕ 6–38˚ selection.

The CDG intensities using standard CDG data selections are listed in table VI.E.3. The 1.8–2.7 MeV effective-area for ϕ 6–38˚ P23a data is 13.45 cm^2-sr Although the average ToF-peak count rate for ϕ 6–38˚ selection is 4.4 times higher than the ToF-peak count rate for ϕ ≥ 22˚, the resulting CDG count rates are consistent with each other, the difference being less than 1 σ. The ^{24}Na- and the ^{24}Na+^{28}Al-subtracted 1.8–2.7 MeV VGC for P23a ϕ 6–38˚ is shown in figure VI.E.5. The CDG flux was also determined by subtracting the 2.6 MeV peak and the 2000-2400 keV excess from the 1.8–2.7 MeV counts. Recall that ~70% of the 2.6 gaussian counts are present in 1.8–2.7 MeV in ETOT. The results are once again consistent (table VI.E.3).

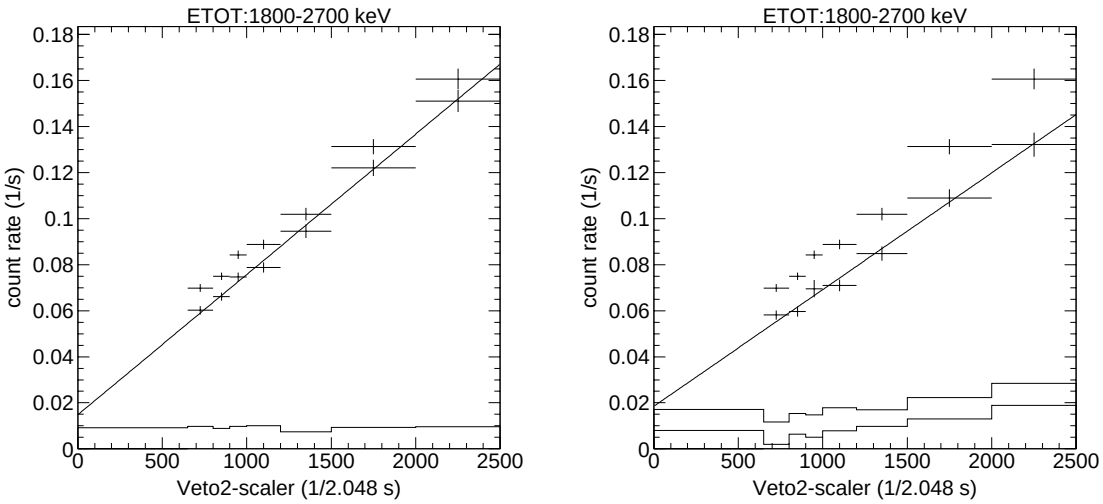

(a) (b)

Figure VI.E.5 The 1.8–2.7 MeV for ϕ 6–38˚ selection with (a) only ^{24}Na-subtracted and, (b) with ^{24}Na+^{28}Al-subtracted from the ToF-peak VGCs prior to extrapolation.

Table VI.E.3 The results for 1.8–2.7 MeV CDG analysis using P23a data with ϕ 6–38°

CDG Extrapolation method	Rate (1/s)	Flux $\times 10^{-3}$ (1/cm^2-s-sr-MeV)
(ToF-peak–^{24}Na) VGC	0.0148 ± 0.0026	1.22 ± 0.21
(ToF-peak–^{24}Na–^{28}Al) VGC	0.0185 ± 0.0031	1.53 ± 0.26
(ToF-peak–^{24}Na–^{28}Al–2.6G–2-2.4excess) VGC	0.0137 ± 0.0041	1.13 ± 0.34

VI.F. The 0.8–1.8 MeV CDG Analysis

The background line components present in the 0.8–1.8 MeV region in ETOT are from ^{22}Na, ^{40}K and the 1.41 MeV line in the E2 spectrum. In addition there are tails from ^{24}Na, ^{28}Al and ^{2}H components. For the 0.8–1.8 MeV range, the analysis is similar to that of the 1.8-2.7 MeV energy range. We first determine the ToF-peak rates using the one gaussian ToF model that includes the contribution from line components within the ToF-peak rates. Then the characteristic decay lines in the individual detector spectrum are fitted to calculate and eventually subtract their contributions to the ToF-peak rates. The long-lived background corrected ToF-peak VGCs are then extrapolated to zero veto rate to determine the CDG count rate. Since the 2.2 MeV line is a prompt background source, its contribution is automatically corrected during the veto extrapolation.

VI.F.1 The E2 Spectral Fit

To minimize the background intensity, the CDG analysis was performed on P23a data with standard CDG data selections. The procedure used here to determine the is identical to that described in section V.C. Figure VI.E.1(a) shows the P23a E2 spectrum together with the exponential function representing the continuum background. Figure VI.E.1(b) shows the exponential-subtracted E2 spectrum that represents the sum contributions of the line emission.

Performing a stepwise line fit from high to low energies in the E2 provides line intensities in the E2 spectrum. The fit includes the identified isotopes and the unidentified components at the 2.94, 2.58 and 1.41 MeV photopeaks together with 2000–2400 keV excess. The E2 line spectrum with each fitted line component and the residuals are shown in figure VI.F.1.

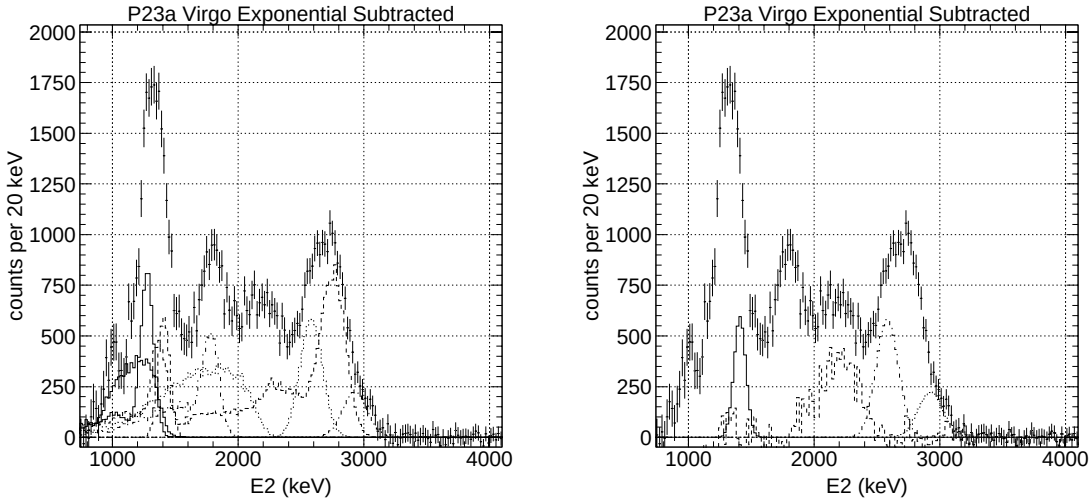

(a) (b)

Figure VI.F.1 The E2 line spectrum with (a) the fitted individual line components ;and (b) the residuals after subtracting all known isotopes.

The VGCs for the line components

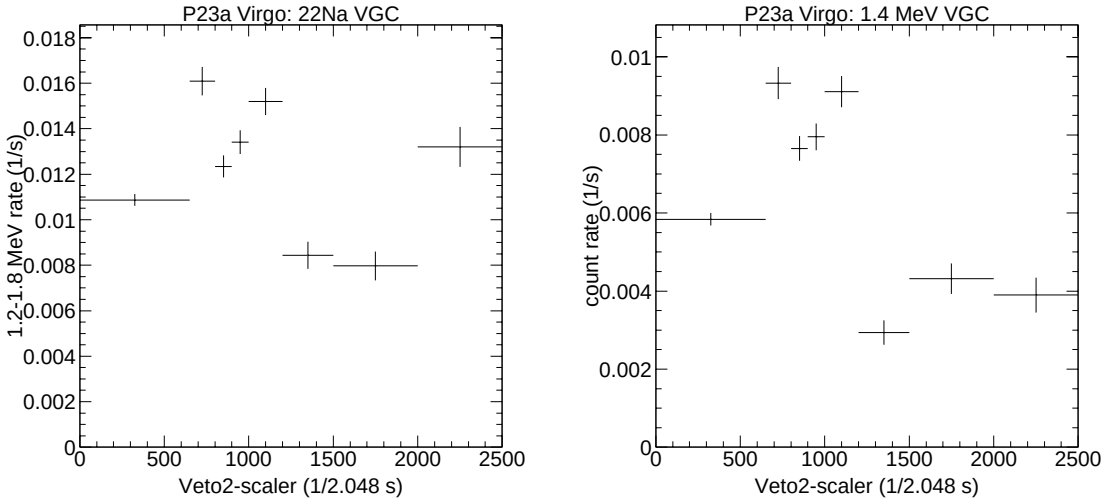

(a) (b)

Figure VI.F.2 (a) The ^{22}Na VGC and (b) the 1.4 MeV VGC for P23a with standard-CDG selections in the 1.2–1.8 MeV bin. The average rate is plotted in the v2: 0–650 bin.

Such E2 spectral fits are performed on each the veto-binned E2 spectra to compute the individual line intensities as a function of the veto2 rate to produce their respective VGCs. The VGCs for ^{24}Na and ^{28}Al were presented earlier (see figures VI.D.3 and VI.E.3). Recall

that ^{40}K is a steady source of background. The VGCs of the ^{22}Na and the 1.4 MeV line in the E2 spectrum are plotted in figure VI.F.2.

VI.F.2 The 1.2–1.8 MeV Flux Calculation

The 0.8–1.8 MeV flux calculation begins by computing the VGCs for each of the line components in the 0.8–1.8 MeV ETOT range. Figure V.C.27 shows the E2 spectrum with the ETOT selection of 1.2–1.8 MeV. The distribution of events for $\phi > 22^{\circ}$ is also plotted. It demonstrates that the 1.4 MeV feature in the E2 spectrum contributes to the 1.2–1.8 MeV counts in ETOT. Subtract all the line components from the 1.2–1.8 MeV ToF-peak VGC. As before, the long-lived background-corrected ToF-peak VGCs are then extrapolated to zero veto-rate to determine the CDG count rate in the 0.8–1.2 and 1.2–1.8 MeV ranges.

The true shape of the ToF fit function is not known. Either a quadratic or an exponential function can be used to represent the ToF continuum. Although the exponential model predicts a 20% higher average count rate above 2 MeV, the extrapolated CDG count rates from both these models are consistent with one another (see section VI.G), but below 2 MeV, these models differ by 40–50%. These large differences result in a major uncertainty in the CDG flux below 2 MeV. Since neither model is necessarily superior, results for both models are presented here. More discussion on the ToF fit function and the differences due to the two methods is presented in section V.A. The fitted ToF spectrum using the two different ToF-fit models in 1.2–1.8 MeV is shown in figure VI.F.3.

As mentioned before, a ToF-correction factor is necessary to account for the events outside the 110–130 ToF window that contribute to the ToF gaussian peak. An estimate of the fraction of line events lost due to the cut is determined from the fitted ToF-peak in ETOT. The ToF exponential model results in ToF-peak position at 119.0 with a width of 5.6 channels; corresponding to a correction of 1.085. The ToF quadratic model results in ToF-peak position at 119.5 with a width of 5.1 channels; corresponding to a correction of 1.054.

The 1.2–1.8 MeV VGC for all three ToF components with their respective straight line fits for the two ToF-fit models are plotted in figure VI.F.5. Note the difference in gaussian amplitudes (P4 in figure VI.F.3) of the two models due to the two fit functions.

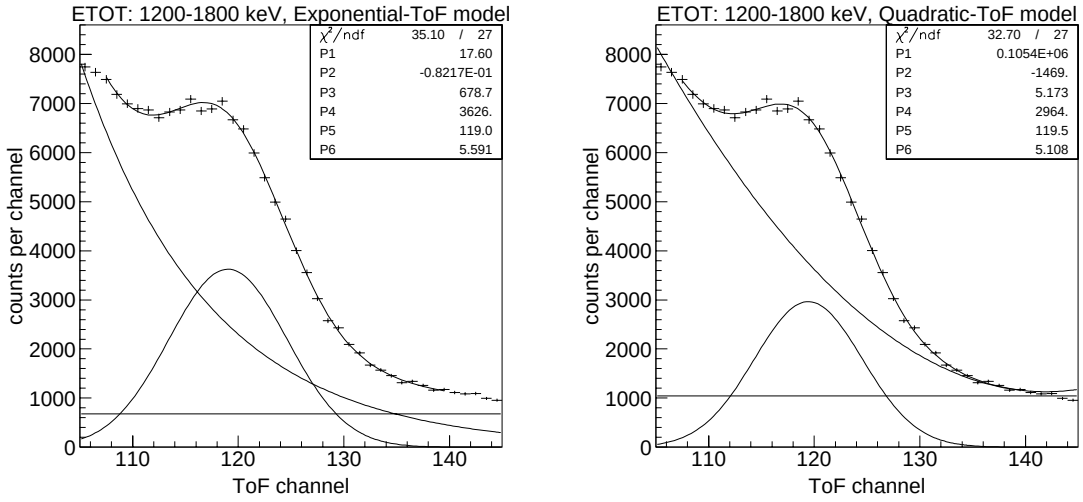

(a) (b)

Figure VI.F.3 The 1.2–1.8 MeV ToF spectrum fit with (a) the ToF-exponential model and (b) the ToF-quadratic model.

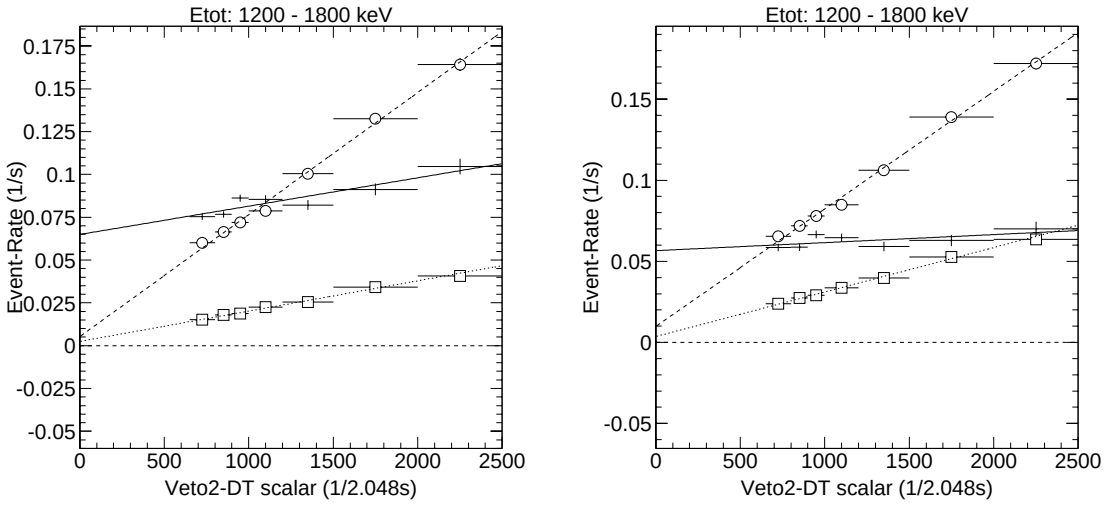

Figure VI.F.4 The 1.2–1.8 MeV VGC for all three ToF components with their respective straight line fits for the two ToF fit models (+: gaussian; square: constant; circle: exponential).

The long-lived background (^{22}Na, ^{40}K, ^{24}Na, ^{28}Al, 1.4 MeV line in E2) subtracted 1.2–1.8 MeV VGC for P23a using standard CDG selections is shown in figure VI.F.5 for the two ToF fit models. The VGC extrapolation results are presented in table VI.F.1. The table also includes the contributions averaged over all veto-rates for each of the line components. The long-lived background dominates the 1.2–1.8 MeV ToF-peak rates with an average

contribution of 49%. The prompt component contributes 31%. The 1.2–1.8 MeV CDG S/B ratio is 20% with a VGC modulation factor of 1.99.

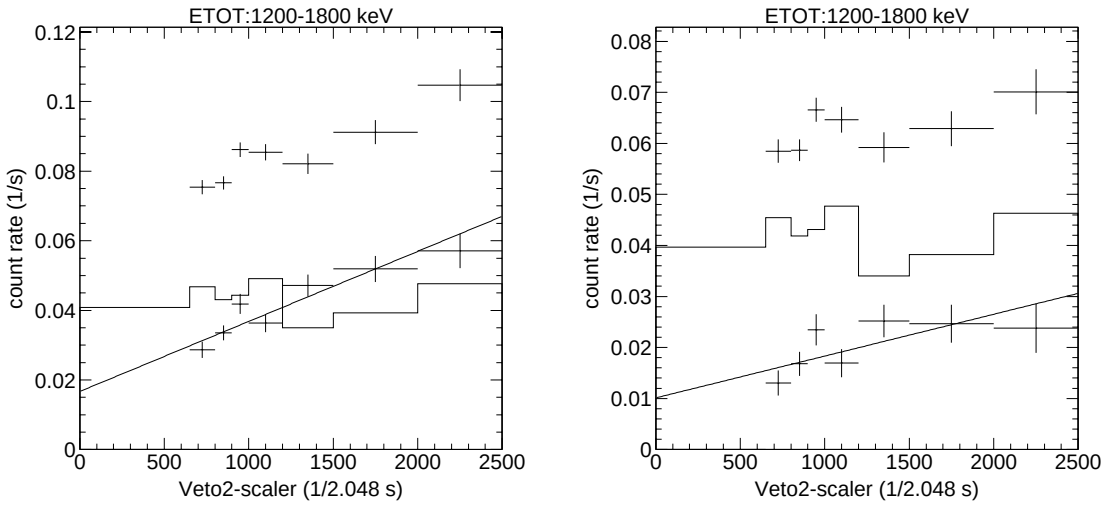

Figure VI.F.5 The line subtracted 1.2–1.8 MeV VGC for P23a using standard CDG selections is shown for the two ToF fit models.

The extrapolated rate at zero veto rate using the ToF-exponential model after all long-lived background corrections is the CDG count rate in the 1.2–1.8 MeV bin. With a CDG count rate of 0.017 ± 0.003 (1/s) and the effective-area with the corresponding data selections of 11.4 (cm^2-sr), the CDG flux value in the 1.2–1.8 MeV range is 0.0024 ± 0.0005 (photons/cm^2-s-sr-MeV). The 1.2–1.8 MeV CDG measurement has a 5.3σ statistical significance. The ToF-quadratic model gives a 1.2–1.8 MeV CDG flux of 0.0015 ± 0.0005 (photons/cm^2-s-sr-MeV). The systematic errors in this energy range are large due to the uncertainties in the ToF fit models and from the long-lived background corrections.

Table VI.F.1 Results for the 1.2–1.8 MeV CDG analysis using P23a data with standard CDG data selections.

Average Rates —		
^{24}Na		0.00750 ± 0.00027
^{28}Al		0.00438 ± 0.00056
^{22}Na		0.01087 ± 0.00027
1.4 MeV gaussian.		0.00584 ± 0.00016
^{40}K		0.01224
sum lines		0.04084
ToF-Exponential model		
ToF-correction		1.085
Avg. ToF-peak rate	(1/s)	0.0834 ± 0.0016
LLB rate/ Avg. rate	(%)	48.9
Prompt rate/ Avg. rate	(%)	31.0
(ToF-peak – LLB) VGC —		
VGC M_v		1.99
VGC slope	(1/s-veto2)	(2.01 ± 0.28) e-5
S/B: CDG rate/ Avg. rate	(%)	20.0
CDG (constant) rate	(1/s)	0.017 ± 0.003
Effective Area	(cm^2.sr)	11.43
CDG flux	(1/cm^2-s-sr-MeV)	0.00243 ± 0.00046
ToF-Quadratic model		
ToF-correction		1.054
Avg. ToF-peak rate	(1/s)	0.0623 ± 0.0021
CDG rate	(1/s)	0.0101 ± 0.0033
CDG flux	(1/cm^2-s-sr-MeV)	0.00148 ± 0.00048

Consistency check for the 1.2–1.8 MeV CDG analysis method

It was argued that a ϕ 22–38˚ selection in the 1.8 to 4.2 MeV analysis suppressed the line contributions resulting in a higher S/B ratio for the CDG signal. A disadvantage of this ϕ selection in the 1.2–1.8 MeV range is that we do not know how to correctly scale the 1.41 MeV photopeak counts to the ϕ 22–38˚ range. Secondly, the decrease in ToF-peak rates with ϕ 22–38˚ of 2.92 is similar to the decrease in the effective area 2.34 implying there is little improvement in the S/B ratio. For these two reasons, we use the standard CDG selections to determine the 1.2–1.8 MeV CDG flux

Nevertheless we can check for consistency in our results by calculating the CDG flux for ϕ 22–38˚ by assuming that the 1.41 MeV line rate scales like that of ^{22}Na when going from a ϕ 6-38˚ to ϕ 22-38˚ selection. Since these two components may have similar D1 and D2 energy deposits this seems reasonable.

The results are presented in table VI.F.2 and figure VI.F.6 for the ToF-exponential model only. The long-lived background subtracted 1.2–1.8 MeV VGC for P23a using ϕ 22–38˚ selections is shown in figure VI.F.7 for the ToF-exponential fit model. The CDG flux in 1.2–1.8 MeV for ϕ 6–38˚selection, 0.00243 ± 0.00046 (1/cm^2-s-sr-MeV) is consistent with the results from the ϕ 22–38˚ selection, 0.00190 ± 0.00049 (1/cm^2-s-sr-MeV).

Table VI.F.2 Results for the 1.2–1.8 MeV CDG analysis using P23a data with ϕ 22–38˚ selection and the Exponential-ToF model.

Effective Area	(cm^2-sr)	4.89
ToF-peak rate	(1/s)	0.0286 ± 0.0007
(ToF-peak – LLB) VGC —		
CDG rate	(1/s)	0.0056 ± 0.0014
CDG flux	(1/cm^2-s-sr-MeV)	0.00190 ± 0.00049

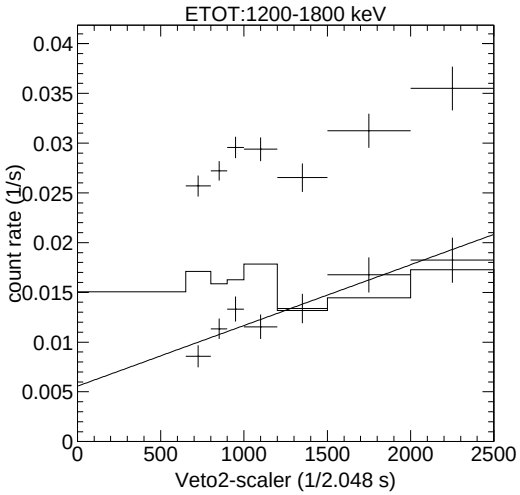

Figure VI.F.6 The line subtracted 1.2–1.8 MeV VGC for P23a with ϕ 22–38˚ selection using the ToF-exponential model.

VI.F.3 The 0.8–1.2 MeV CDG Flux Calculation

The 0.8–1.2 MeV CDG analysis is similar as for the 1.2–1.8 MeV range. All of the long-lived components discussed to this point contribute to this bin (with the exception of the 2.6 and 3.0 MeV lines in E2). All the VGCs have been previously determined and their counts have been calculated for the 0.8–1.2 MeV bin.

The fitted ToF spectrum with both ToF models are shown in figure VI.F.7. Note the difference in gaussian amplitude (P4 in figure VI.F.7) between the two models due to the difference in the two fit functions. The ToF exponential model results in ToF-peak position at

119.7 with a width of 6.25 channels; corresponding to a ToF correction factor of 1.124. The ToF quadratic model results in ToF-peak position at 120.4 with a width of 5.42 channels; corresponding to a correction factor of 1.070.

The 0.8–1.2 MeV VGC for all three ToF components with their respective straight line fits are plotted in figure VI.F.8 for the two ToF fit models. The long-lived background corrected 0.8–1.2 MeV VGC for P23a using standard CDG selections is shown in figure VI.F.9 for both ToF-fit models. The results for VGC extrapolation are presented in table VI.F.3. The table also includes the average contributions of each the line components to the count rate. The long-lived background and the prompt component contribute 22% and 31% to the average ToF-peak rates, respectively. The 0.8–1.2 MeV CDG S/B ratio is 47% with a VGC modulation factor of 1.24.

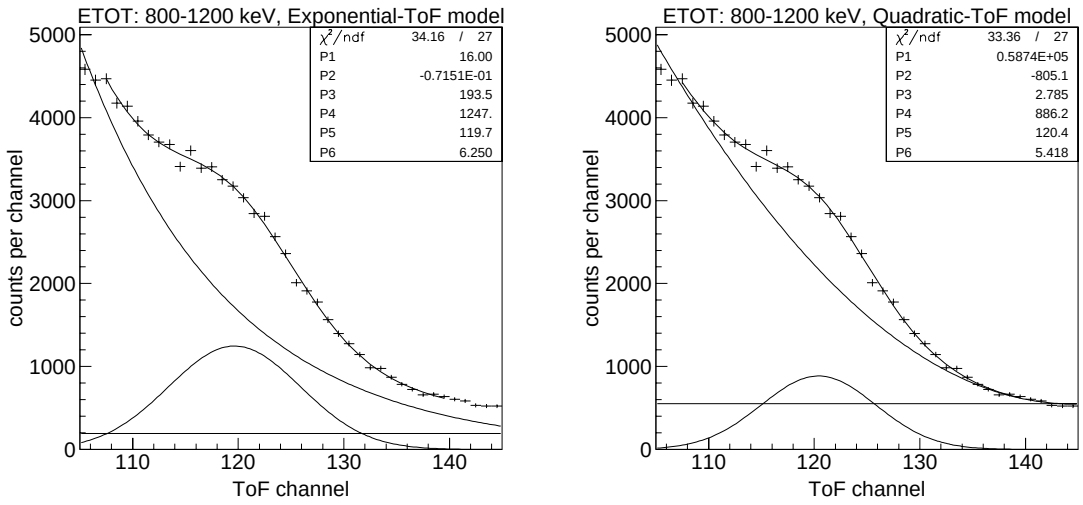

(a) (b)

Figure VI.F.7 The 0.8–1.2 MeV ToF spectrum fit with (a) the ToF-exponential model and (b) the ToF-quadratic model.

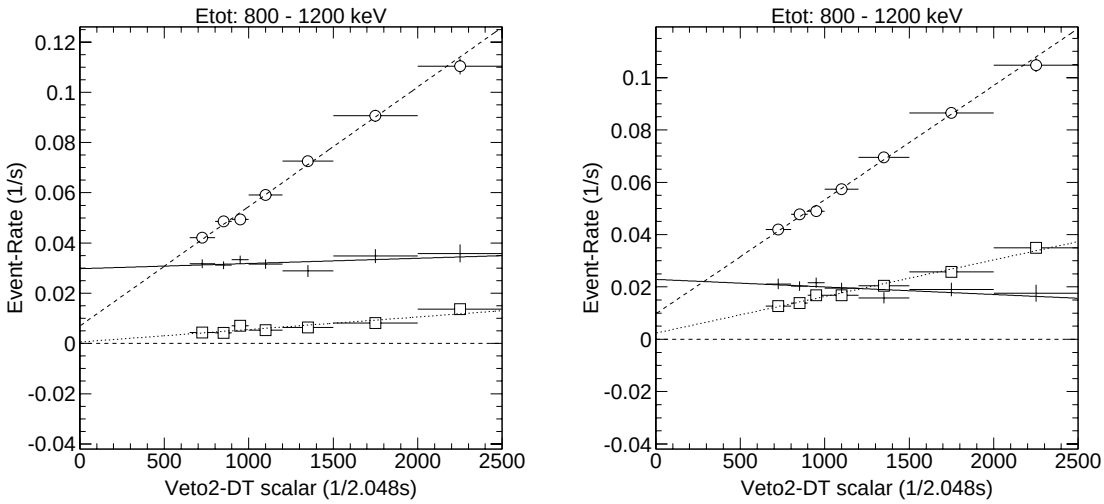

Figure VI.F.8 The 0.8–1.2 MeV VGC for all three ToF components with their respective straight line fits for the two ToF fit models (+: gaussian; square: constant; circle: exponential).

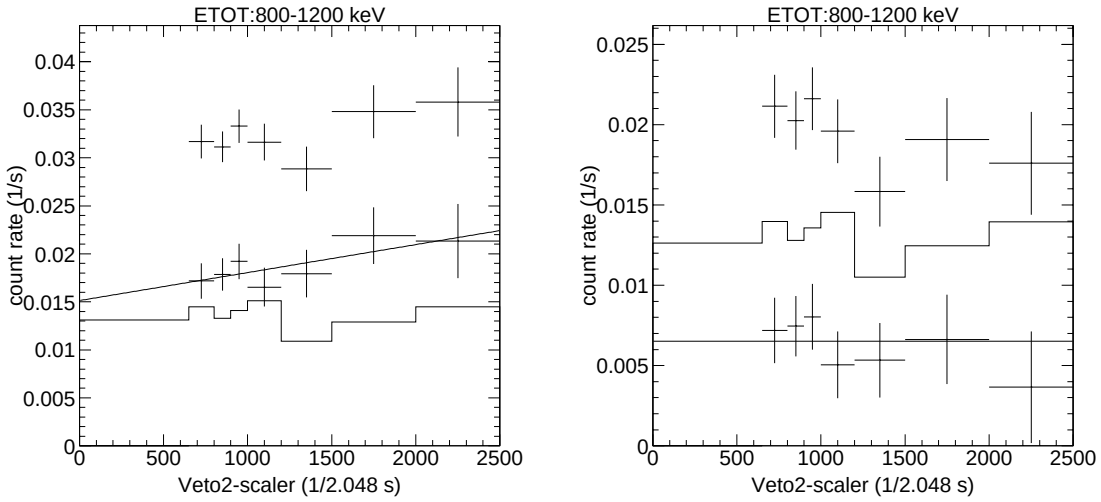

Figure VI.F.9 The line subtracted 0.8–1.2 MeV VGC for P23a using standard CDG selections for the two ToF fit models.

Table VI.F.3 Results for 0.8–1.2 MeV CDG analysis using P23a data with standard CDG selections.

Averaged Rates —		
^{24}Na		0.001488 ± 0.000054
^{28}Al		0.000706 ± 0.000090
^{22}Na		0.001822 ± 0.000045
1.4 MeV gaussian		0.000979 ± 0.000027
^{40}K		0.002086
sum lines		0.007081
ToF-Exponential model		
ToF-correction		1.124
ToF-peak rate	(1/s)	0.0321 ± 0.0012
LLB rate/ Avg. rate	(%)	22.1
Prompt rate/ Avg. rate	(%)	30.7
(ToF-peak – LLB) VGC —		
VGC M_v		1.24
VGC slope	(1/s-veto2)	(2.9 ± 2.2) e-6
S/B: CDG rate/ ToF-peak rate	(%)	47.2
CDG (constant) rate	(1/s)	0.0151 ± 0.0025
Effective Area	(cm^2-sr)	5.82
CDG flux	(1/cm^2-s-sr-MeV)	0.0065 ± 0.0011
ToF-Quadratic model		
ToF-correction		1.070
ToF-peak rate	(1/s)	0.0198 ± 0.0020
CDG rate	(1/s)	0.0065 ± 0.0009
CDG flux	(1/cm^2-s-sr-MeV)	0.0028 ± 0.0004

The extrapolated rate at zero veto-rate after all long-lived background corrections using the exponential-ToF model gives a CDG count rate of 0.0151 ± 0.0025 (1/s) in the 0.8–1.2 MeV bin. With an effective area of 5.82 (cm^2-sr) for the corresponding data selections the CDG flux in the 0.8–1.2 MeV bin is 0.0065 ± 0.0011 (photons/cm^2-s-sr-MeV). The 0.8–1.2 MeV CDG measurement has a 6.02σ statistical significance. The quadratic-ToF model gives a 0.8–1.2 MeV CDG flux of 0.0028 ± 0.0004 (photons/cm^2-s-sr-MeV). As before the systematic errors in this energy range are large due to the uncertainties in the ToF fit models and from the long-lived background corrections.

As in the 1.2–1.8 MeV energy bin, the ϕ 22–38˚ selection does not result in a significant increase in the 0.8–1.2 MeV S/B ratio (the effective area decreases by 1.70 while the ToF-peak rate decreases only by 1.61), therefore we use the standard CDG selections with ϕ 6–38˚ to determine the 0.8–1.2 MeV CDG flux.

VI.G. Systematic Error Calculation

In this chapter we describe the method used to determine the systematic errors in the CDG data analysis. Due to the nature of the background, the analysis method and the data selections vary with energy. In addition to the statistical errors, there are additional uncertainties in our results due to the method itself. For example, an exponential function is used to describe the ToF continuum function, but the continuum can also be described with a quadratic as discussed in section V.A. The differences in the results of these models are systematic in nature and are not reflected in the statistical error. In general, systematic errors are difficult to estimate.

There are five major sources of systematic error in the CDG analysis. They originate from (1) the uncertainty in the ToF fit function; (2) the choice of veto dome used to produce the VGCs; (3) the VGC extrapolation method; (4) the long-lived activation calculation; and (5) the CDG instrument response. Each of these sources is discussed individually and the corresponding systematic error is computed for each energy bin.

VI.G.1 The ToF Fit Function

The true shape of the ToF continuum beneath the ToF forward-peak is not known. It can be adequately modeled by either an exponential or a quadratic function. However, both these functions fail if they are used to describe the spectrum far (~15 ToF channels) from the gaussian peak at channel 120. One less parameter is required to determine the constant component if one uses the exponential ToF-continuum function. The exponential function systematically predicts higher counts in the ToF-peak at all energies (20% above 2 MeV and 40% below 2 MeV).

To address the question, “How do the systematic differences in the ToF peak rate affect the calculation of the CDG event rate?” We have calculated the CDG flux for all energy bins using both ToF-fit functions with their respective optimized CDG data selections. The VGCs for each CDG energy bin are plotted in figures VI.G.1–9. The exponential function prior to extrapolation uniformly assigns higher count rates to the gaussian component. The higher rates are seen for all energies and at all veto bins.

Table VI.G.1 shows the resulting CDG rates from both ToF-fit functions. The values are for P23a data for E <4.2 MeV and P15VSGP data for E >4.2 MeV with optimized-CDG data selections in each energy range. The fractional differences and the significances of the differences are also tabulated. The fractional difference is the difference between the two rates over the average rate. The significance of the difference is the ratio of the difference over the statistical error.

Above 1.8 MeV, the differences in the rates are less than 0.5σ with no systematic trend. The fractional differences are in the 5–25% range. The CDG rates from both ToF fits are consistent with each other. The systematic differences are always smaller than the statistical uncertainties. The VGC extrapolation seems to be properly account for the 20% difference in absolute rates due to the different ToF-fit functions. Below 1.8 MeV, the differences for the CDG flux from the two models are much larger (40–55%). Clearly, the systematic uncertainties dominate other uncertainties.

The difference between the resulting CDG fluxes when using the two ToF-fit functions are also tabulated. It is this difference in the predicted flux that we use as an estimate of the systematic error introduced by the choice of the ToF-fit function.

Table VI.G.1 Systematic errors from the ToF-fit function.

Energy (MeV)	CDG Rate Quad-ToF (1/s)	CDG Rate Exp-ToF (1/s)	Change in Rate (%)	Change in Rate (σ)	Change in CDG flux ($1/cm^2$-s-sr-MeV)
0.8–1.2	0.00652 ± 0.00085	0.0151 ± 0.0025	–79.5	5.12	0.003697
1.2–1.8	0.01013 ± 0.0033	0.0167 ± 0.0031	–49.0	1.99	0.000957
1.8–2.7	0.0043 ± 0.0011	0.0044 ± 0.0010	–1.54	0.06	1.84×10^{-5}
2.7–4.2	0.00128 ± 0.00070	0.00129 ± 0.00065	–0.6	0.01	1.33×10^{-6}
4.2–6	0.00081 ± 0.00036	0.00062 ± 0.00022	26.4	0.76	2.09×10^{-5}
6–9	0.00038 ± 0.00019	0.00035 ± 0.00016	9.2	0.19	2.70×10^{-6}
9–12	0.00065 ± 0.00013	0.00062 ± 0.00013	3.9	0.19	7.49×10^{-7}
12–17	0.00050 ± 0.00010	0.000521 ± 0.000099	–4.7	0.24	5.11×10^{-7}
17–30	0.000233 ± 0.000083	0.000203 ± 0.000075	13.9	0.38	4.16×10^{-7}

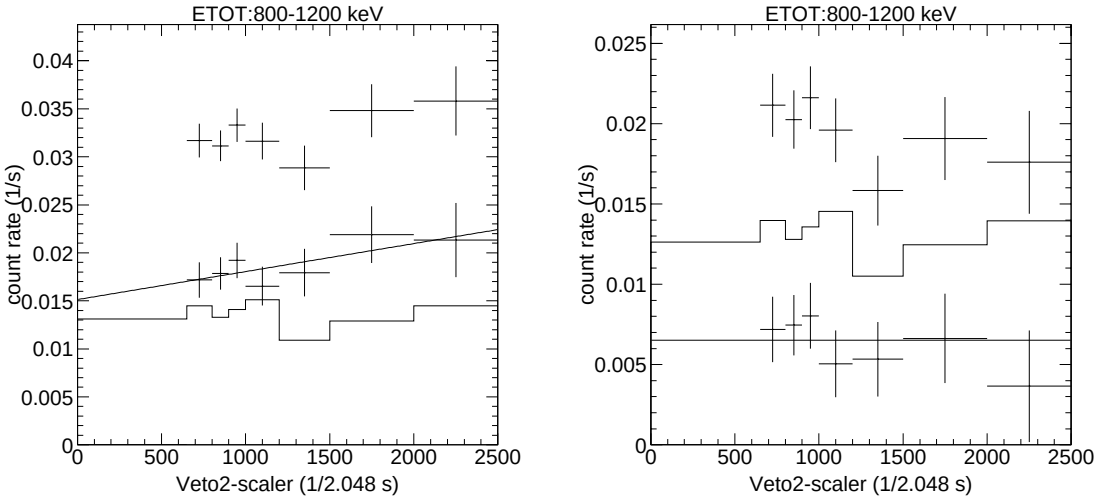

Figure VI.G.1 0.8–1.2 MeV: Comparison between the CDG count rates derived using a quadratic-ToF function (right) and an exponential-ToF function (left).

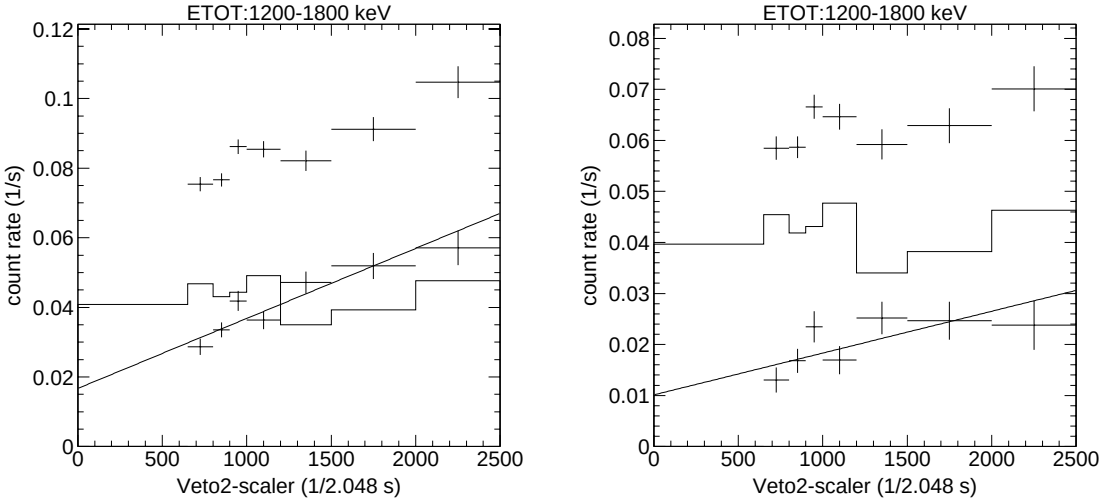

Figure VI.G.2 1.2–1.8 MeV: Comparison between the CDG count rates derived using a quadratic-ToF function (right) and an exponential-ToF function (left).

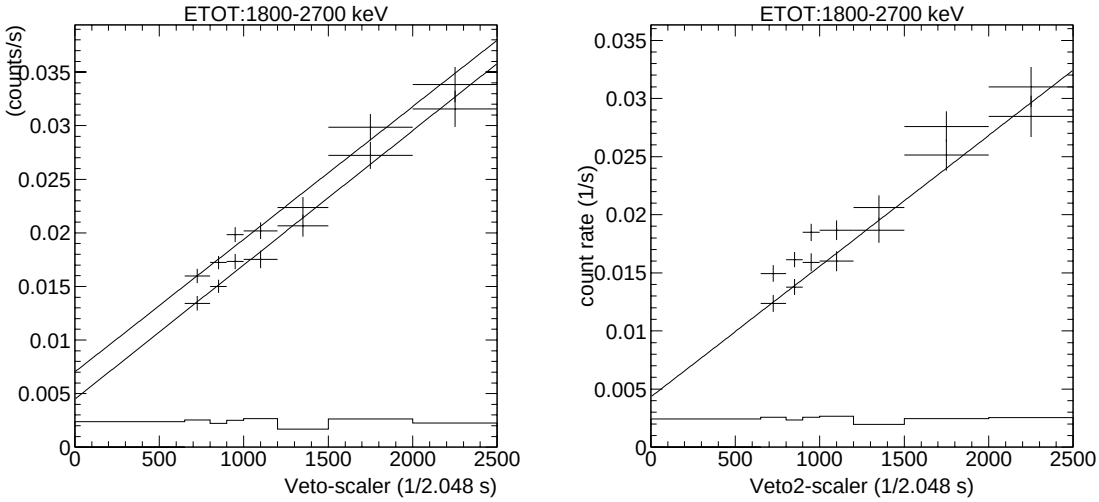

Figure VI.G.3 1.8–2.7 MeV: Comparison between the CDG count rates derived using a quadratic-ToF function (right) and an exponential-ToF function (left).

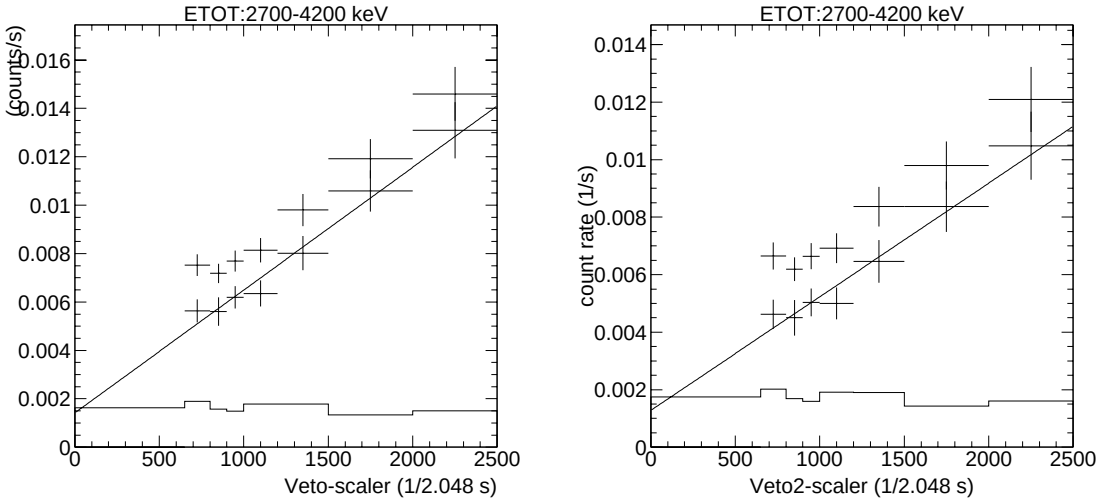

Figure VI.G.4 2.7–4.2 MeV: Comparison between the CDG count rates derived using a quadratic-ToF function (right) and an exponential-ToF function (left).

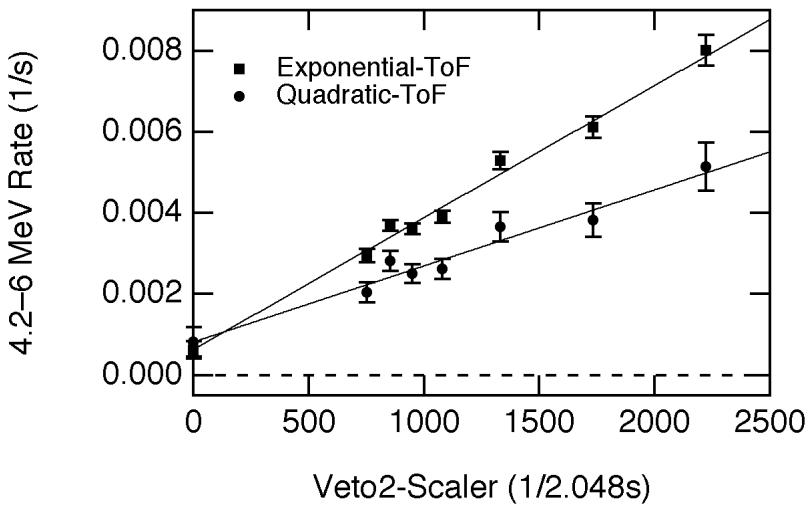

Figure VI.G.5 4.2–6 MeV: Comparison between the CDG count rates derived using a quadratic-ToF function (right) and an exponential-ToF function (left).

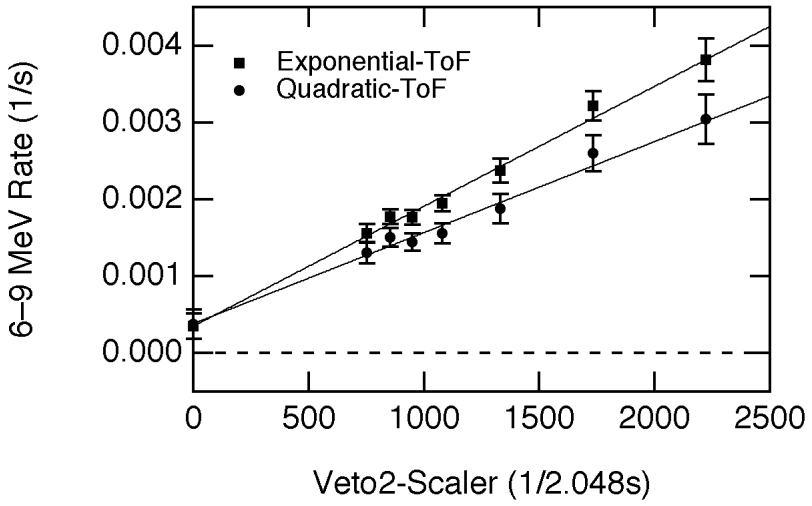

Figure VI.G.6 6–9 MeV: Comparison between the CDG count rates derived using a quadratic-ToF function (right) and an exponential-ToF function (left).

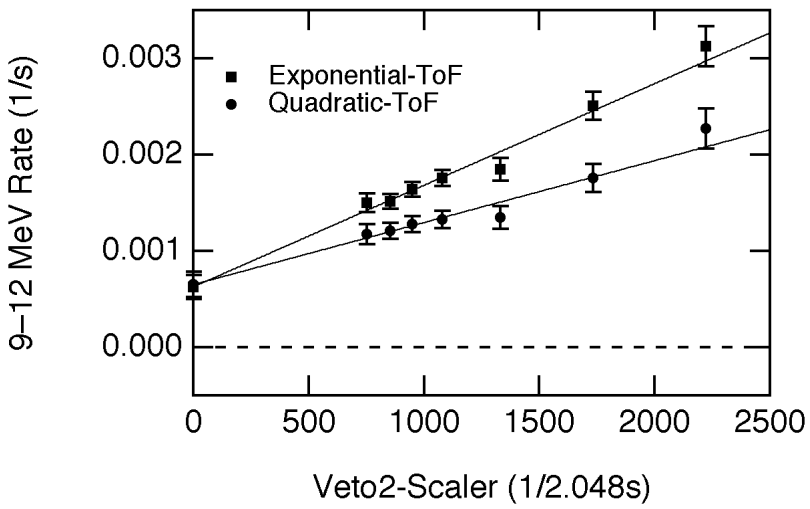

Figure VI.G.7 9–12 MeV: Comparison between the CDG count rates derived using a quadratic-ToF function (right) and an exponential-ToF function (left).

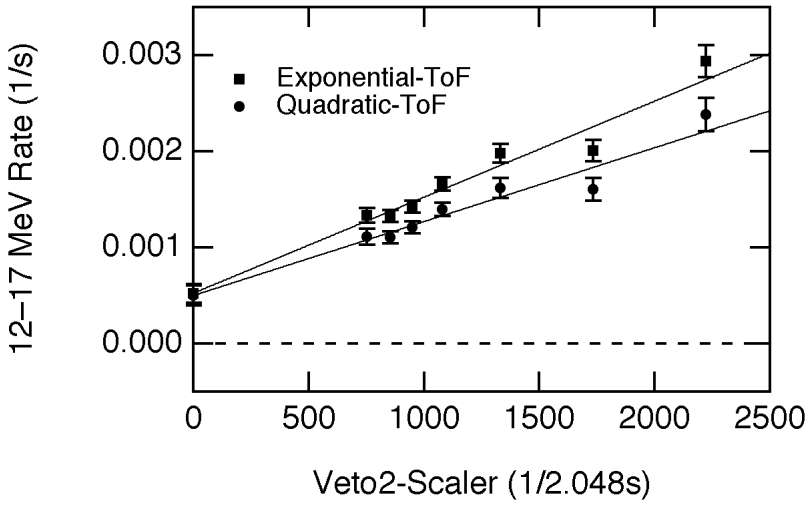

Figure VI.F.8 12–17 MeV: Comparison between the CDG count rates derived using a quadratic-ToF function (right) and an exponential-ToF function (left).

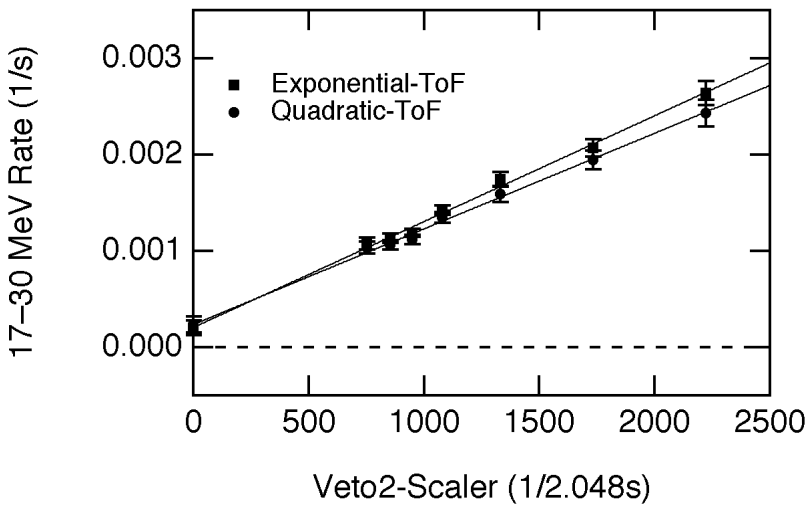

Figure VI.G.9 17–30 MeV: Comparison between the CDG count rates derived using a quadratic-ToF function (right) and an exponential-ToF function (left).

VI.G.2 The VGC Extrapolation

The strong 2.223 MeV instrumental line has been used as a diagnostic for all prompt background sources. Since the 2.2 MeV line is a prompt background component, we expect all prompt background components to have a similar dependence on the veto rates or the local cosmic-ray intensity. The key results from the study of the 2.2 MeV behavior (see section V.E) are that (1) the 2.2 MeV rate is fairly constant over 5 years of COMPTEL operations and (2) the 2.2 MeV rate is proportional to the veto rate. The second point implies that the 2.2 MeV rate linearly vanishes at zero veto rate or that the prompt background in general vanishes at zero veto rate. This assumption of the prompt background vanishing at zero veto rate is incorporated into the CDG analysis when we extrapolate the ToF-peak VGC with a straight line (after correcting for any long-lived background) to determine the baseline level (*y*-intercept) which is then assigned to the CDG radiation.

As part of the study, the 2.2 MeV VGCs were fit by a straight line to determine the best fit *y*-intercept. These *y*-intercepts were found to be consistent with zero. Nevertheless, we use the *y*-intercept to determine the veto rate (*x*-intercept) for which the measured 2.2 MeV rate is zero. Assuming that all prompt background vanishes at this non-zero veto-rate, the CDG intensities are determined by extrapolating to this non-zero veto rate. By comparing the CDG intensities from extrapolating to this non-zero veto rate to that derived from extrapolating to zero, we get a measure of the sensitivity of the CDG flux to veto-rate extrapolation.

The Virgo and SGP combined dataset (P15VSGP), with the best statistics, give a value of 29 ± 67 for the veto2-offset rate, consistent with zero. To get a measure of the fluctuations in the CDG flux due to the uncertainties in extrapolating to zero veto2 rate, the CDG flux was computed assuming a veto2-offset rate of 67. The changes to the CDG flux are tabulated in table VI.G.4 and can be interpreted as an estimate of the systematic error associated with extrapolating the prompt background to zero using the veto2 detector. The systematic differences are always smaller than the statistical uncertainties with significances always less than 1σ. The fractional differences are typically 10–20% where the worst case for the 4.2–6 and 17–30 MeV bins where the error increases to ~35%.

The differences in the CDG flux due to a non-zero veto2 rate depends on the slope of the VGC. As the slope increases the fractional contribution of the CDG emission to the overall rate decreases. For a given offset veto rate, the steeper the slope the larger the difference due to the offset. The error estimate is sensitive to the magnitude of the VGC extrapolation: the property an error for the VGC extrapolation should exhibit. Thus, using the non-zero veto2 rate (veto2 = 67) to compute changes to the CDG flux gives a good measure of the systematic error associated with the veto extrapolation.

Table VI.G.2 Systematic errors from VGC extrapolation.

Energy (MeV)	CDG Rate @ zero v2-rate (1/s)	VGC slope (1/s-veto2)	CDG Rate @ 67 v2-rate (1/s)	Change in Rate (%)	Change in Rate (σ)	Change in CDG flux ($1/cm^2$-s-sr-MeV)
0.8–1.2	0.0151	2.92e-6	0.0153	1.29	0.08	8.4e-5
1.2–1.8	0.0167	2.01e-5	0.0180	8.08	0.43	1.97e-4
1.8–2.7	0.00439	1.25e-5	0.00523	19.10	0.80	2.30e-4
2.7–4.2	0.00129	5.09e-6	0.00163	26.52	0.53	6.5e-5
4.2–6	0.000622	3.26e-06	0.000840	35.07	0.99	2.41e-5
6–9	0.000347	1.56e-06	0.000452	30.13	0.65	8.50e-6
9–12	0.000624	1.06e-06	0.000695	11.33	0.56	2.13e-6
12–17	0.000522	9.99e-07	0.000589	12.84	0.68	1.43e-6
17–30	0.000203	1.10e-06	0.000277	36.31	0.98	1.01e-6

VI.G.3 The Veto Dome Dependence

COMPTEL has four independent veto domes that each measure a charged particle trigger (veto) rate. The CDG analysis was done using the veto-2 data to generate the VGCs. However one could also produce the VGCs by using the rates of the other veto domes. We do not expect there to be any large differences between the veto-domes because (1) all four of the

domes are triggered by the same cosmic-ray flux and the difference between their measured rates conform to the difference in the domes sizes; and (2) the rates between the four veto domes are linearly related to one another (see discussion in section V.D).

We can verify the above hypothesis by explicitly computing the VGCs using the other veto dome data, and comparing their VGC behaviors. The extrapolations using the different dome data were performed only for the P3V data. The VGCs are computed for the 4.2–9 and 9–30 MeV bins using the optimized CDG data selections in each energy bin. The 4 VGCs and their respective fits are shown in figures VI.G.10 and VI.G.12 for the 9–30 and 4.2–9 MeV bins, respectively. The *y*-intercept (CDG intensities) for the two energy bins using the four different domes are also plotted separately in figures VI.G.11 and VI.G.13 and listed in table VI.G.3.

The VGC slopes for the four domes are different since their scalar ranges are different while the range of measured count rates are the same for the different domes. The VGC intercepts (CDG intensity) from the different domes are consistent with each other (see figures VI.G.11 and VI.G.12). The reduced chi-square for a straight line fit to the CDG rates are 0.308/3 and 0.0507/3 for the 4.2–9 and 9–30 MeV bins, respectively. There are no large variations introduced in the CDG measurement by using any one dome for the CDG extrapolation. The variations in the CDG intensities due to the different domes are much smaller than their statistical errors. Hence the veto2 data is as good as any other veto dome data for the purpose of VGC extrapolation. The original motivation for choosing veto2 was that it was relatively better shielded within the instrument and hence less likely to be triggered by photons or other secondary charged particles produced in the spacecraft.

Table VI.G.3 Systematic errors from the choice of a veto-dome rate.

Veto Dome	4.2–9 MeV CDG Rate with 2gToF+ϕ>18° (1/s)	9–30 MeV CDG Rate with 1gToF+ϕ>6° (1/s)
1	- 0.00025 ± 0.00063	0.00073 ± 0.00042
2	- 0.00019 ± 0.00061	0.00082 ± 0.00035
3	- 0.00013 ± 0.00064	0.00081 ± 0.00043
4	0.00019 ± 0.00061	0.00086 ± 0.00042
mean rate	- 0.000095 ± 0.00031	0.00081 ± 0.00020
1σ rate	0.000197	0.000054
1σ flux	8.82 × 10-6	2.78 × 10-7

We can now compute the variance of the CDG flux using the four veto domes. This variance can be interpreted as a measure of the systematic error introduced by using any one particular veto dome for the CDG extrapolation: veto2 in our case. The weighted mean, the 1σ error (square-root of the variance) and the corresponding 1σ flux (in 1/cm^2-s-sr-MeV) are also tabulated in the table VI.G.3.

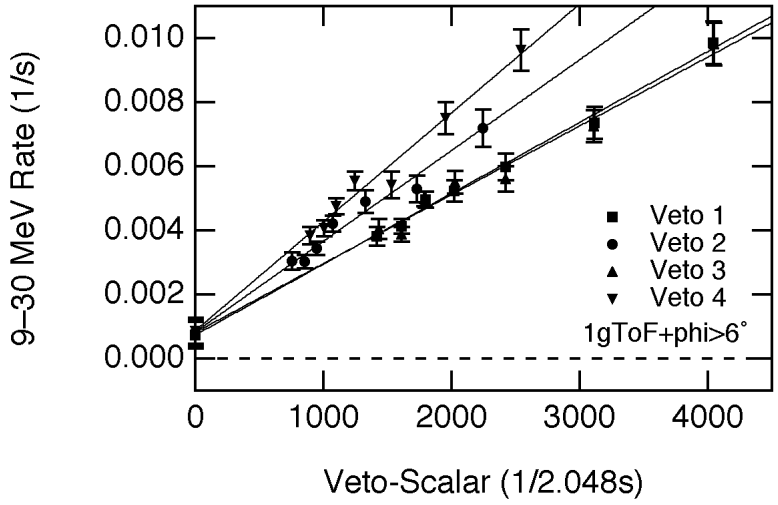

Figure VI.G.10 The 9–30 MeV ToF-peak VGCs generated using the four veto-domes.

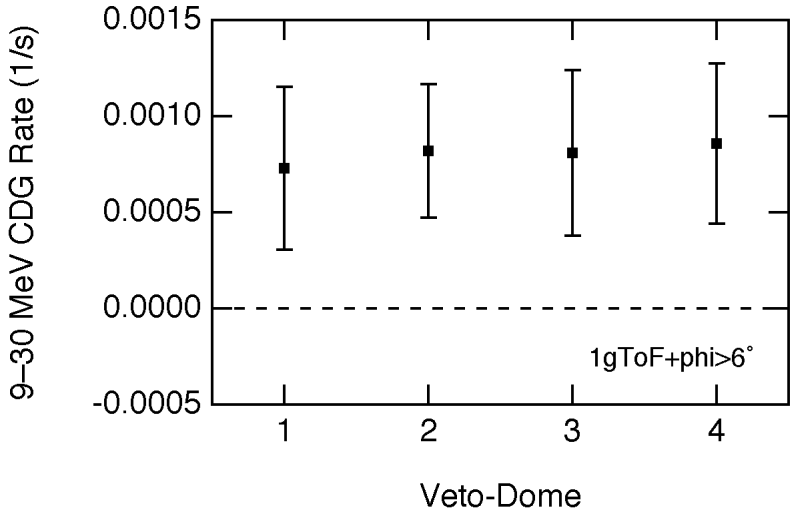

Figure VI.G.11 The 9–30 MeV CDG count rate using the four veto-domes.

Unfortunately, it is not possible to compute a fractional error by this method. These errors are available for only the 4.2–9 and 9–30 MeV region. Since these errors are relatively the small, ignoring their contributions to the other energy ranges does not significantly affect the total systematic error calculation.

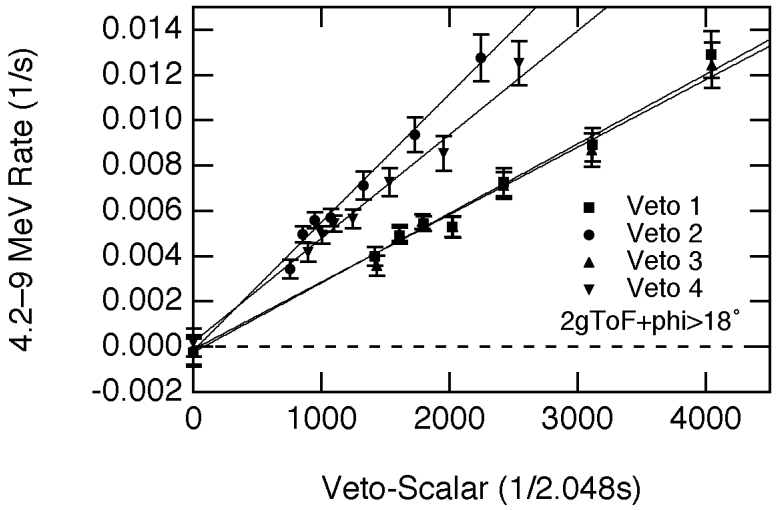

Figure VI.G.12 The 4.2–9 MeV ToF-peak VGCs generated using the four veto-domes.

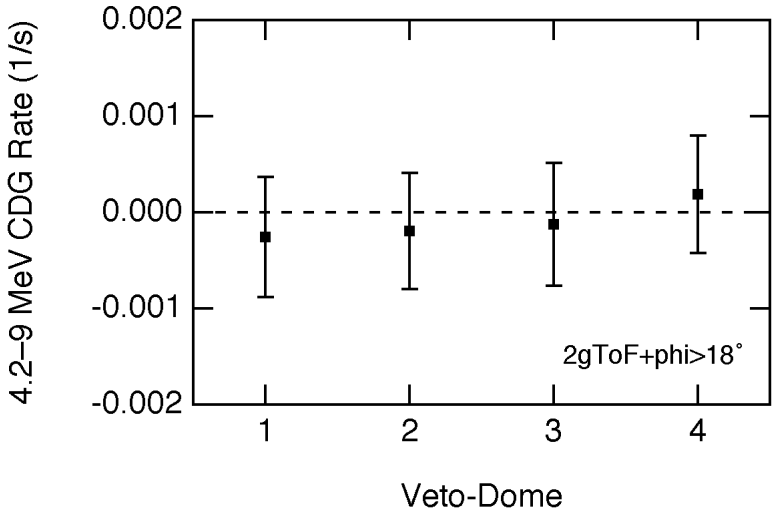

Figure VI.G.13 The 4.2–9 MeV CDG count rate using the four veto-domes

VI.G.4 The Long-Lived Background Subtraction

There are possible systematic uncertainties associated with the fitting of the lines. The statistical uncertainties of the fitted intensities are properly folded through in computing their intensities and their subtraction. In section VI.D on the 2.7–4.2 MeV CDG analysis, I fitted the ^{24}Na with the Na24-E1 cut so as to enhance the 2.754 peak with respect to the continuum. The ^{24}Na was also fit for standard data selections.

The 25% difference in the ^{24}Na intensities using these two methods gives an approximate measure of the systematic uncertainties in the ^{24}Na intensity. By computing the flux

corresponding to 25% uncertainty in the long-lived background correction in each of the CDG bins, we can get an estimate of the systematic errors associated with the subtraction of long-lived activation. The errors are listed in table VI.G.4. This procedure gives a higher systematic error to those bins with large long-lived background corrections: the property long-lived background subtraction error should exhibit.

Table VI.G.4 Systematic errors from long-lived background subtraction.

Energy (MeV)	CDG Rate @ zero v2-rate (1/s)	Veto-averaged LLB rate (1/s)	25% LLB (1/s)	flux ($1/cm^2$-s-sr-MeV)
0.8–1.2	0.0151 ± 0.0025	0.0070	0.00177	0.00076
1.2–1.8	0.0167 ± 0.0031	0.0408	0.01021	0.00149
1.8–2.7	0.0044 ± 0.0011	0.0024	0.00060	0.00016
2.7–4.2	0.0013 ± 0.0006	0.0016	0.00041	0.000078

VI.G.5 The CDG Response Calculation

There are no practical calibrations that can measure the COMPTEL response to an isotropic gamma-ray source. Hence, a Monte Carlo simulation system (SIM) based on the CERN-GEANT package is used to compute the instrument response for the general case of a diffuse source. The package uses a detailed model of the COMPTEL mass distribution and the measured instrument characteristics during calibration such as the individual module energy thresholds, the PSD response and the positional smear to determine the instrument response to the incident photon flux.

One measure of the error in the effective area (response) comes from the Poisson error associated with the number of photons simulated after all the relevant data selections are applied. By simulating sufficiently large number of photon events this Poisson error can be reduced to any desired level. The Poisson error associated with the CDG effective area calculation ranges from 1–3.5%. However this Poisson error does not take in account the uncertainties in the simulation mass distribution or the errors in the empirically determined instrument characteristics. Therefore, a value of 15% has been adopted as a generous estimate of the systematic errors in the CDG energy response for all CDG energy bins.

VI.G.6 Summary of Systematic Errors

The table VI.G.5 below summarizes all the systematic sources discussed above and quotes the total systematic error by adding the individual systematic errors in quadrature.

Table VI.G.5 The total systematic error for each energy bin.

Energy (MeV)	ToF-model	Veto-ext.	Effec-Area	LLB-sub	veto2	total-error
	(1/cm^2-s-sr-MeV)					
0.8–1.2	0.003697	8.4e-5	9.75e-4	7.60e-4		3.90e-3
1.2–1.8	0.000957	1.97e-4	3.65e-4	1.49e-4		1.05e-3
1.8–2.7	1.84×10^{-5}	2.30e-4	1.81e-4	1.64e-4		3.36e-4
2.7–4.2	1.33×10^{-6}	6.5e-5	3.57e-5	7.77e-5		8.55e-5
4.2–6	2.09×10^{-5}	2.41e-5	1.05e-5		8.82e-6	3.47e-5
6–9	2.70×10^{-6}	8.50e-6	4.76e-6		8.82e-6	1.34e-5
9–12	7.49×10^{-7}	2.13e-6	2.82e-6		2.78e-7	2.93e-6
12–17	5.11×10^{-7}	1.43e-6	1.67e-6		2.78e-7	2.27e-6
17–30	4.16×10^{-7}	1.01e-6	4.16e-7		2.78e-7	1.20e-6

The total systematic error is dominated by different sources depending on the energy range. For example, the 0.8–1.2 and 1.2–1.8 MeV region are most influenced by the ToF fits. From 1.8–4.2 MeV the veto-rate extrapolation, the long-lived background correction and the effective-area errors are all comparable. Above 4.2 MeV the two main sources of error are from the veto-rate extrapolation and effective-area uncertainties. The energy dependence of systematic error on different background sources is compatible with the model of the physical background. With the exception of the lowest two energy bins the systematic errors are comparable to the statistical uncertainties.